D180-30550-3

Final Report

Task 4 - Impact Detection/Location System

SPACE STATION INTEGRATED WALL DESIGN AND PENETRATION DAMAGE CONTROL

By

J. M. Nelson and B. M. Lempriere

Prepared for

National Aeronautics and Space Administration

July 1987

Contract NAS8-36426

Technical Management
NASA George C. Marshall Space Flight Center
Marshall Space Flight Center, Alabama
Structures and Dynamics Laboratory
Sherman L. Avans

Boeing Aerospace Company
Seattle, Washington

D180-30550-3

Final Report

Task 4 - Impact Detection/Location System

SPACE STATION INTEGRATED WALL DESIGN AND PENETRATION DAMAGE CONTROL

By

J. M. Nelson and B. M. Lempriere

ABSTRACT

This report documents a program to develop a methodology for detecting and locating meteoroid and debris impacts and penetrations of a wall configuration currently specified for use on Space Station. Testing consisted of penetrating and non-penetrating hypervelocity impacts on single and dual plate test configurations, including a prototype 1.22 m x 2.44 m x 3.56 mm (4 ft x 8 ft x 0.140 in) aluminum waffle grid backwall with multi-layer insulation and a 0.063-in shield. Acoustic data were gathered with transducers and associated data acquisition systems and stored for later analysis with a multi-channel digitizer. Preliminary analysis of test data included sensor evaluation, impact repeatability, first waveform arrival, and Fourier spectral analysis.

KEY WORDS

Acoustic Emission

Hypervelocity Impact

Impact Detection

Impact Location

Space Station

Spectral Analysis

Transducers

Waveforms

CONTENTS

FIGURES

This page left intentionally blank.

1.0 INTRODUCTION

The concern for meteoroid and orbital debris impact on Space Station has led to a need for locating perforations when these are small and hidden, allowing speedy repairs. A preliminary experiment conducted in 1986 on BAC IR&D showed that acoustic emission sensors would provide a practicable means of collecting data from the impact response of a panel, and a simple algorithm was able to determine the impact location with satisfactory precision. This led to an add-on to this existing NASA/MSFC contract to further investigate the detection of impacts.

The present effort has been devoted to evaluating the limitations of the method from the point of view of designing a system with a minimum number of sensors and evaluating the possibilities that information on damage to the panel and on the speed and nature of the impactor could be derived from the impact waveforms.

The objectives of the program were to:

1. Determine the accuracy of measurements to be used for locating meteoroid impact to allow design trades with respect to numbers of sensors and computing capability,

and

2. Evaluate the potential for determining the extent of impact damage and characteristics of the impactor from the transient bending response of the panel.

This page left intentionally blank.

2.0   APPROACH

Signals detected by acoustic emission sensors at various distances from small impacts on a sheet of aluminum and a sample Space Station panel were recorded. The data were processed to evaluate:

1.   The accuracy of locating the impact in relation to the accuracy of first-arrival measurement,

2   The effects of frequency-dependent dispersion of wavefronts causing errors in first-arrival times,

3.   The feasibility of determining propagation distance by using the Fourier phase spectrum and the dispersive spectral characteristics of bending motions,

4.   The feasibility of inferring changes in bending characteristics and thus inferring the occurrence of damage by using feature analysis, and

5.   The feasibility of deducing the impact velocity from the pulse magnitude and the impactor size from the pulse duration.

PRECEDING PAGE BLANK NOT FILMED

This page left intentionally blank.

3.0 IMPACT TESTS

3.1 TEST MATRICES

Matrices showing the sequence of tests that have been conducted are shown in figures 3.1-1 through 3.1-3. Preliminary tests were made on a 1.22m x 1.83m x 4.76-mm (4-ft x 6-ft x 3/16-in) thick aluminum panel. The impactor was a copper clad steel or nylon BB from a common BB gun. A sample of the machined Space Station waffle panel was used for a brief series of penetration tests under high velocity impact from a powder gun. The purpose of each test and a discussion of the test progression follows the matrix. The results are presented and discussed below.

The preliminary tests were made using two wide-band acoustic emission sensors with a two-channel digitizer. A multi-channel device was later acquired to enable the recording of signals from several transducers on each test.

The impact time is not measured in a real system where the impact location is not known, so it would be deduced by the location algorithm from the waveforms. To provide additional data for evaluating the algorithm, a large low-frequency (100 KHz) ultrasonic transducer was placed under the impact point in several tests to provide an impact time fiducial.

3.2. COMMENTS ON TEST SEQUENCE

The first three tests of 01/21 were made to examine changes, with distance, in the waveforms between two sensors spaced apart in a line. They were placed at 102-mm (4-in) and at 254-mm or 381-mm (10-in or 15-in) from the impact. Waveforms for the three tests are shown in Appendix A as figure A-1. The waveforms at 102-mm (4-in) and those at 254-mm (10-in) are quite similar to each other, indicating repeatability. The 254-mm (10-in) waveforms exhibit the expected dispersion (spreading of the pulse to lower frequency at longer time), but their amplitudes were not the same. One of these waveforms (IMP2) has been subjected to considerable processing, as discussed under Results.

PRECEDING PAGE BLANK NOT FILMED

FIGURE 3.1-1 PRELIMINARY TESTS

Date	Data Id	Sensor Distance from Impact (ins)					Measured Velocity (ft/sec)
		#1	#2	#3	#4	#5	
Dispersion Data							
01/21/87	IMP1.DAT	4	10	-	-	-	-
"	IMP2.DAT	4	10	-	-	-	-
"	IMP3.DAT	4	-	15	-	-	-
02/10/87	IMPACT.DAT	3	-	7	-	-	-
"	"	3	-	7	-	-	-
"	"	3	5	-	-	-	-
"	"	3	5	-	-	-	-
"	"	3	-	-	10	-	-
"	"	3	-	-	10	-	-
Impact Velocity Data							
03/05/87	0306.AE	3	-	-	10	0	293.3
03/06/87	"	3	-	7	-	0	285.3
"	"	3	5	-	-	0	285.8
Evaluate Transducer #4							
03/20/87	0320.AE	12	-	-	12	0	279.0
"	"	12	-	-	12	0	279.0

FIGURE 3.1-2 MULTI-CHANNEL FIXED DISTANCE DATA

Date	Data Id	Sensor Distance from Impact (ins)					Measured Velocity (ft/sec)
		#1	#2	#3	#4	#5	
03/25/87	0325_1.AE	12	12	12	12	0	270.0
"	0325_2.AE	12	12	12	12	0	268.7
04/01/87	0401.AE	12	12	12	12	0	265.5
04/02/87	0402.AE	12	12	12	12	0	261.6
04/06/87	0406_1.AE	Approx 6 in fr			#1		260.3
"	0406_2.AE	"	3	"	"	#2	260.3
"	0406_3.AE	"	8	"	"	#2	270.2
04/07/87	0407_1.AE	"	5	"	"	#2	268.7

FIGURE 3.1-3 LOCATION TESTS

Date	Data Id	Sensor Distance from Impact (ins) #1 #2 #3 #4 #5	Measured Velocity (ft/sec)
Flat Panel			
(nylon sphere impactor)			
04/14/87	0414_1.AE		520.5
"	0414_2.AE		540.8
"	0414_3.AE		520.2
"	0414_4.AE		526.0
Waffle Panel			
Low Velocity Impact			
(nylon sphere impactor)			
04/20/87	0420_1.AE		536.0
"	0420_2.AE		539.7
"	0420_3.AE		537.8
"	0420_4.AE		538.9
"	0420_5.AE		555.1
"	0420_6.AE		520.4
(Copper clad steel BB impactor)			
04/23/87	0423_1.AE		262.1
"	0423_2.AE		263.4
"	0423_3.AE		256.1
"	0423_4.AE		267.9
"	0423_5.AE		276.9
"	0423_6.AE		258.4
High Velocity Impact			
05/04/87	0504_1.AE		3.10 km/sec
05/04/87	0504_2.AE		3.22 "
05/05/87	0505_1.AE		1.27 "
05/06/87	0506_1.AE		3.30 "

Repeatability between tests was of concern because only two recording channels were available, so distance effects could only be evaluated from data on repeated tests.

The next series of six tests was made on 02/10 to provide data at several distances, with improved experimental techniques. The two transducers for each test were bonded with Loctite, and the launcher was mounted at a fixed distance from the panel. The data for sensors at 125-mm, 178-mm, and 254-mm (5-in, 7-in, and 10-in) (figure A-2) showed expected changes with distance. The data from the near-in reference sensor at 76-mm (3-in) (figure A-3) showed considerable variation in signal strengths and waveforms among the sensors.

The third set of three tests on 03/05 and 06 were instrumented for measuring the impactor velocity to determine whether this could be a source of variation from shot to shot. It was found to be quite repeatable, as shown in figure 3.1-1. The waveforms at 125-mm, 178-mm, and 254-mm (5-in, 7-in, and 10-in) (figure A-4) were similar to those of the previous tests, and those at 76-mm (3-in) were somewhat repeatable.

Three tests of 03/20 were intended to evaluate the transducer used at 254-mm (10-in) because doubt arose as to whether its response was inverted. Two transducers were placed side-by-side at about 305-mm (12-in). The results (figure A-5) showed only moderate differences between them, but both sensors exhibited waveforms that were less characteristic of dispersive bending than in the previous tests. It is thought that the mass of the two together inhibited bending. It could not be clearly established whether there was a sign reversal.

A preliminary test was made on 03/25 using the multi-channel digitizer to compare the signals from four transducers at one distance. Also, a projectile timing device consisting of two screens of fine wire was placed between the gun barrel and the panel to determine whether the gun performance was repeatable. The transducers were placed next to each other on a line perpendicular to a radius from the impact. The signals (figure A-6) were quite similar to each other in the first 100 microseconds or so, but became dissimilar after that as discussed in Results. These waveforms exhibited little bending dispersion, again probably due to the mass of four transducers close together.

Several tests were made on 3/25, 4/1, 4/2, 4/6, and 4/7 using a configuration with four transducers placed at 45-deg intervals around an arc of 305-mm (12-in) radius centered on the impact point. The ultrasonic transducer was used at the impact point to provide a trigger in the first two tests (though its signal was not recorded) but was not installed for the other tests, so triggering was taken from the other transducers. The data are shown in figures A-7 to A-13. The first two of these showed that transducer no. 4 was still suspect, as its signals were low by a factor of 10. Indeed it was found to contain a faulty connector. Problems were encountered with the projectile timing device and were resolved during the sequence of tests. The transducer closest to the impact (no. 2) exhibited unexplained high spikes at an early time in the last three tests.

Four tests were then conducted on 04/14 to obtain data similar to those of the original IR&D effort, but now using multi-channel recording of four transducers arranged in a 305-mm (12-in) square so that all data were simultaneous. The projectile was a 4.0-mm (5/32-in) dia nylon sphere. The data given in figures A-14 and A-15 show lower signals than for the previous tests using the copper-clad steel BB, but apparently with a higher content of high frequency.

Six tests were made on 4/20. Additional transducers were used to investigate alternatives to the acoustic emission sensors. These included a low frequency bending sensor ("Sondicator"), based on a 25-KHz crystal, and a thin piezoelectric film ("Kynar"). Data are shown in figures A-16 to A-21.

Tests on the waffle panel shown in the photo of figure 3.2-1 were begun with six low velocity (BB) shots on 4/23. The sensors were arrayed within the waffle squares to provide transmission directly within a panel as well as across the stiffener ribs. Data are given in figures A-22 to A-27. The signals were widely varied among the transducers, though all showed some of the expected features. Many included high spikes that offset the automatic scaling, but the signal appears normal. The problem is thought to lie in the digitizer, which uses an interpolation procedure to fill in data between sampling times.

High velocity tests were conducted on 5/4, 5/5, and 5/6 using the waffle panel and a two-stage powder gun with cylindrical aluminum pellets. These tests were designed to conform to predictions of penetration made in BAC IR&D studies (reference 1) as represented by the graph of

9
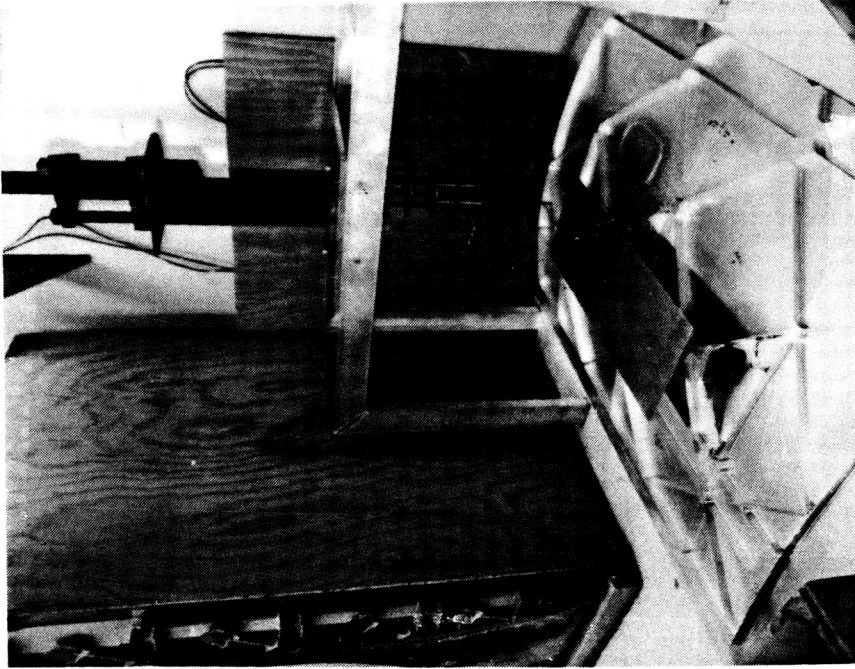
Two stage powder gun and waffle panel with shield attached.
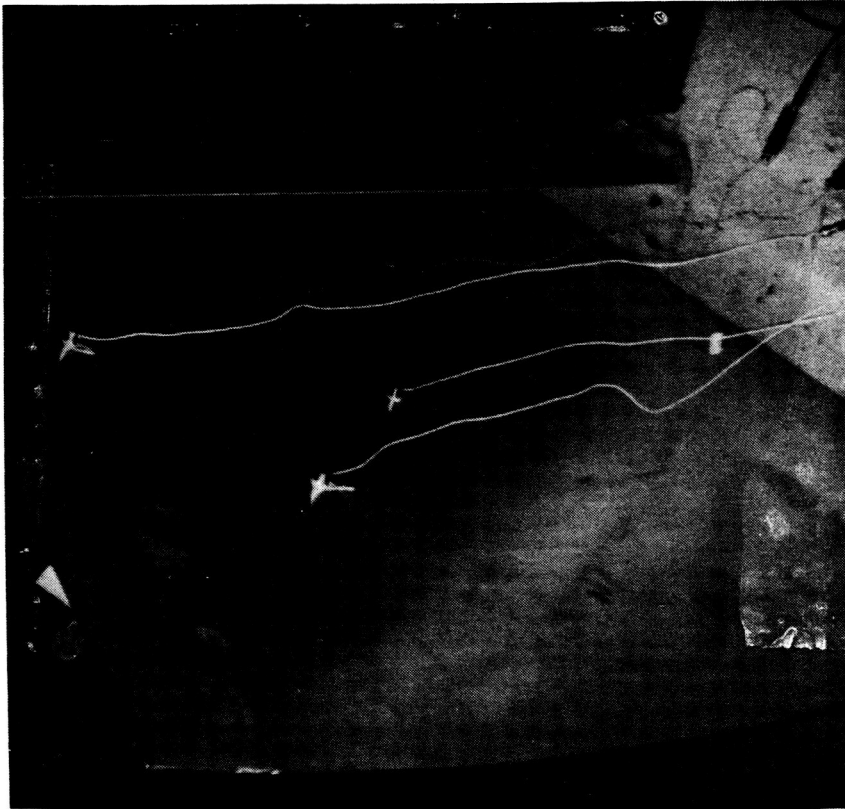
Acoustic emission transducers attached to the panel on the smooth, concave side.

Figure 3.2-1. *Waffle Panel Impact Test Setup for Impact Detection/Location System.*

figure 3.2-2, showing a penetration threshold for projectile diameter and velocity. As indicated, test conditions using the BAC powder gun were selected to provide some penetrating and some non-penetrating shots: one with 6.4-mm (1/4-in) dia pellet at 3 mm/microsecond onto a shield of 0.063-in aluminum, the same with 20 layers of insulation on the panel, the same at 1.5 mm/microsecond, and one with a 3.2-mm (1/8-in) dia pellet at 3 mm/microsecond. The locations of the impact points and sensors on the waffle panel is illustrated in figure 3.2-3. The installation of the shield plate and the multi-layer insulation materials is illustrated in figure 3.2-4.

The first test was unsuccessful as the trigger was incorrectly timed. Further, no penetration occurred when it was expected. The remaining four shots were satisfactory. Signals for these shots are shown in figures A-28 to A-31. Photographs of the impact perforations are shown in figure 3.2-5.
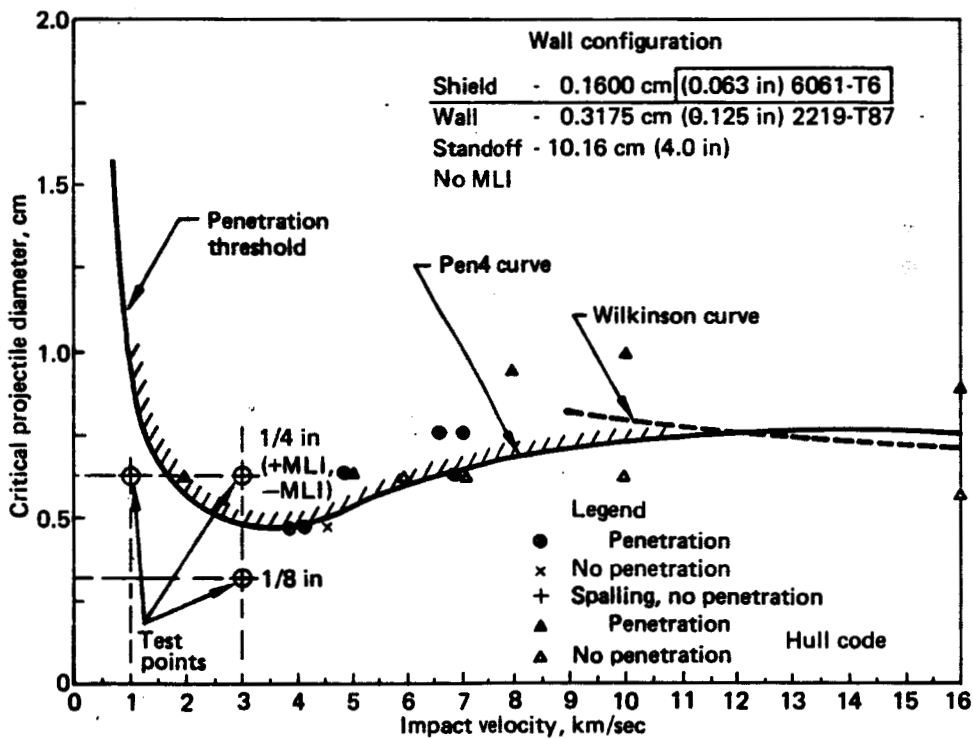
Figure 3.2-2. Selected Test Points Versus Pretest Predictions

Transducer Locations
(4 for each shot)

X Impact Points

I_1 : 0.125 in dia at 3 km/s
I_2: 0.250 in dia at 1 km/s
I_3 : 0.250 in dia at 3 km/s (no MLI)
I_4 : 0.250 in dia at 3 km/s

20 in
TYP

14.25 in
TYP

I_4 X

I_3 X

I_2 X

I_1 X
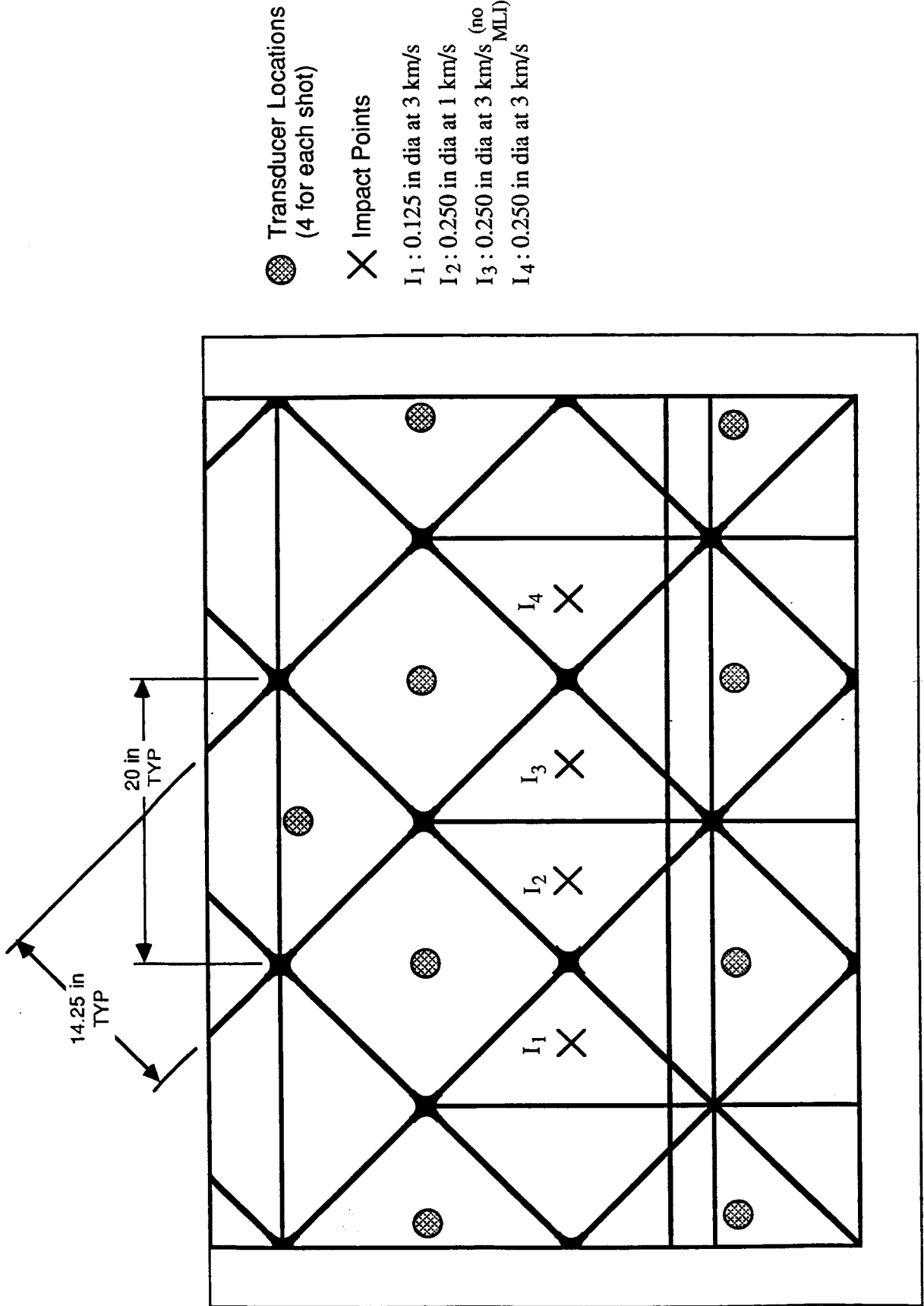
Figure 3.2-3. Waffle Panel Test Arrangement.

12

Multilayer Insulation (MLI)
1 layer beta cloth (outside)
20 layers reinforced insulation
8 in square taped on

Hub in panel

0.25 in dia rod mounting
2 places

4 in
Standoff

X Impact Points
X Re-use shield for
next impact.

Rod mounting
2 places

Shield
26 in X 8 in X 0.063 in
6061-T6 Aluminum
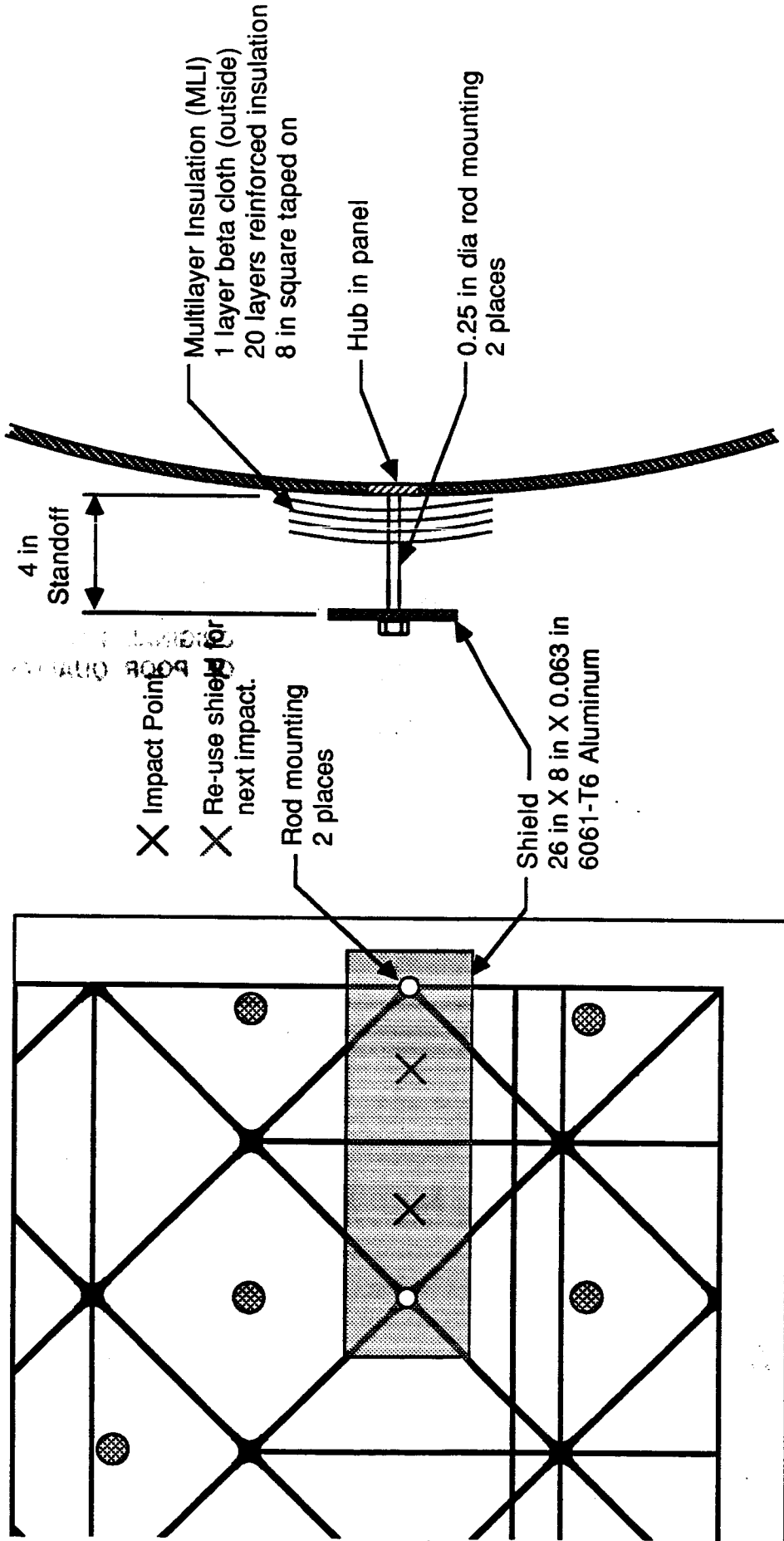
Figure 3.2-4. Installation of Shield and Insulation on Test Panel.

13
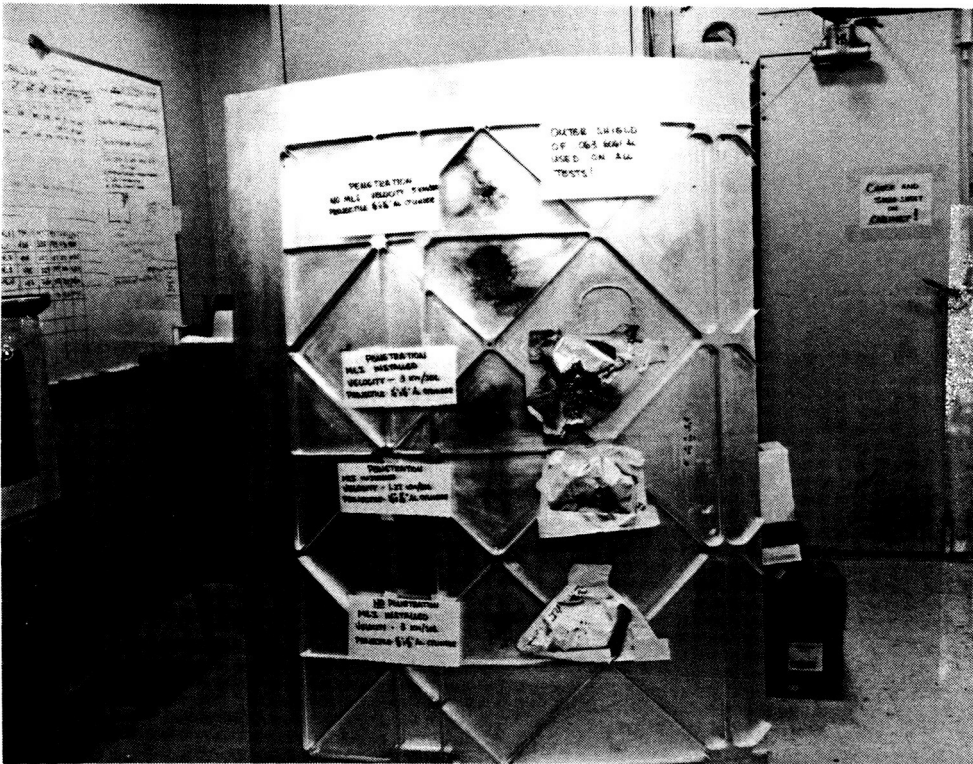
Complete Waffle Panel

**ORIGINAL PAGE IS
OF POOR QUALITY**

Closeup of shot I_3

Figure 3.2-5. Waffle Panel After Hypervelocity Impact

14

4.0   THEORY

4.1   RESPONSE

The dynamic response of a plate takes the form of in-plane and lateral motions. These generally occur in a wide range of modes, having properties of propagating waves with frequency-dependent wavespeeds or of stationary oscillations that do not propagate. Up to moderate frequencies the in-plane response propagates by simple waves having a constant wavespeed known as the plate speed. This is typically slightly less than the dilatational (longitudinal) speed for the material, because the plane stress state caused by lateral relief of stress at the faces of the plate is less stiff than the plane strain state of a plane wave. The transverse response behaves like ordinary bending at low frequency with a diffusion-like character having an apparent[1] speed that varies with the square root of frequency. At high frequency it behaves like Rayleigh surface waves on the two faces of the plate. The relative magnitudes of these various motions are dependent on the loading and the boundary conditions.

4.2   THE GENERAL SOLUTION

Solutions of the differential equations for in-plane motions, $u(x,z,t)$ and lateral motions, $w(x,z,t)$ of a thin plate are found (reference 2) in the propagating exponential forms

$$u = U(z)e^{ik(x-ct)}$$

and

$$w = W(z)e^{ik(x-ct)}$$

These propagate at the wavespeed c and oscillate in time at a frequency $\omega = kc$ with spatial wavenumber k. The thickness variations $U(z)$ and $W(z)$ are determined by two thickness scale factors

$$q = k(1-c^2/c_1^2)^{1/2}$$

---

[1] A motion with such wave speed dependence is not a true wave because the speed of low frequencies approaches zero, and no wave packets of similar frequency can group together as all frequencies have different speed.

and

$$s = k(1-c^2/c_2^2)^{1/2}$$

with c_1 and c_2 being the longitudinal and shear speeds of the material, respectively. These quantities are related by the two equations for:

1) In-Plane:

$$\tanh(sh)/\tanh(qh) = 4sqk^2/(k^2+s^2)$$

and

2) Transverse:

$$\tanh(qh)/\tanh(sh) = 4sqk^2/(k^2+s^2)$$

These are referred to as the dispersion relationships which determine the wavespeed c through q and s as functions of k and thus of ω. Graphical representations are available as illustrated in figure 4.2-1 (from reference 2.)

4.3 IN-PLANE MOTIONS

Up to moderate frequencies, the in-plane motions are governed by the common wave equation, in which the wavespeed is the plate velocity

$$c_{pl} = \{E/\rho(1-v^2)\}^{1/2} = \{(1-2v)^{1/2}/(1-v)\}\ c_L$$

where E is Young's modulus, ρ is the density, v is Poisson's ratio, and c_L is the longitudinal wavespeed for plane waves in unbounded media. For $v = 1/3$, typical of aluminum, the factor is 0.904. Since c_L in aluminum is about 6.3 mm/microsecond, then $c_{pl} = 5.7$ mm/microsecond.

At high frequencies where motions through the thickness become constrained by lateral inertia effects, the waves propagate slower, at the Rayleigh velocity, which for aluminum is $c_R = 3.1$ mm/microsecond.

From a point source, these waves propagate cylindrically, decaying, because of increased area, as the logarithm of distance. Typically this reduces amplitude to negligible levels within 20 to 100 source diameters, about 120- to 600-mm (5- to 25-in) for a 6-mm (1/4-in) impactor.

16

Dispersion curves for the Timoshenko theory and for the
two lowest transverse modes in a slab and in a circular rod
(Poisson's ratio $\nu = 0.29$)
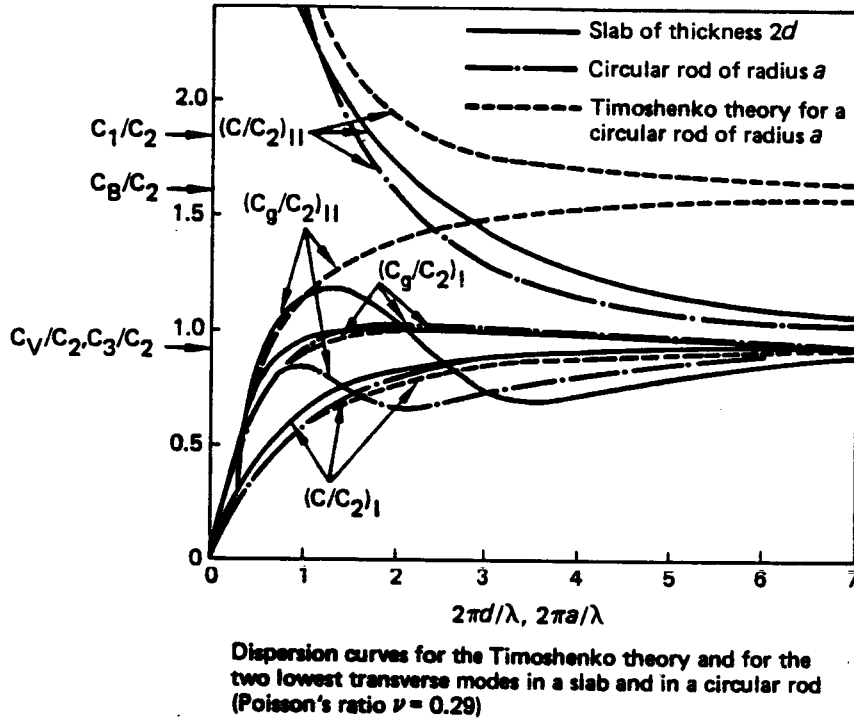
Figure 4.2-1. Calculated Dispersion Curves for a Plate
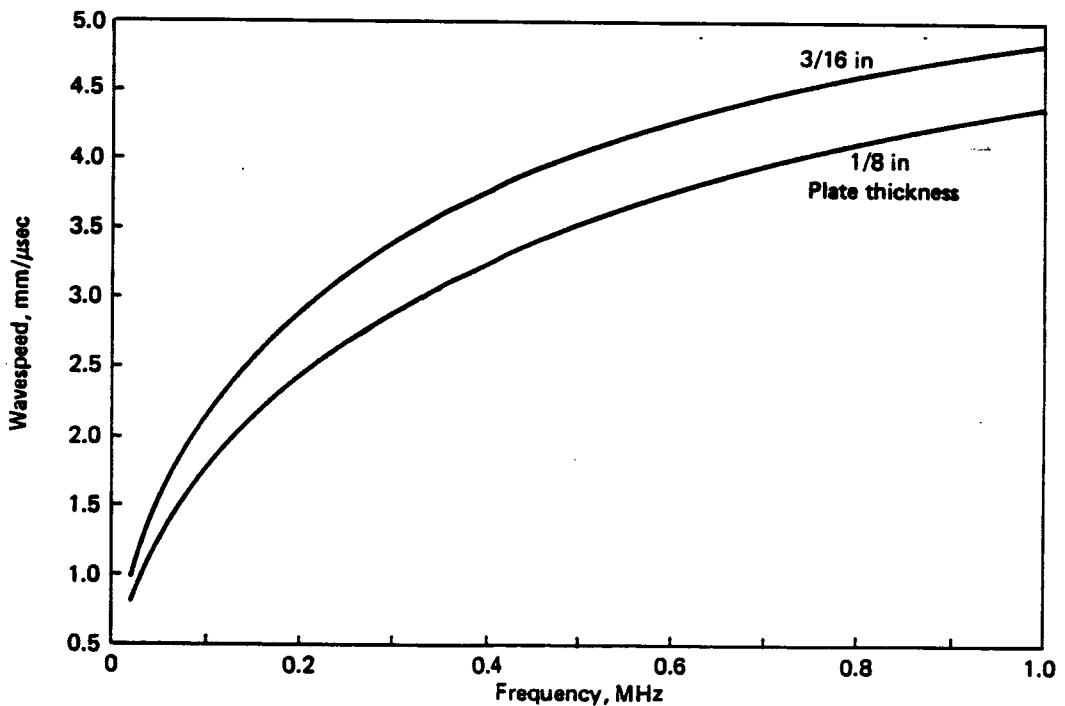
Figure 4.4-1. Calculated Dispersion Curves for Bending of Aluminum Plates of Two Thicknesses

17

4.4 LATERAL (BENDING) MOTIONS

A simplified analysis based on the Timoshenko Beam Theory (reference 3) leads to the approximate but explicit dispersion relationship:

$$k = (\omega/\sqrt{2}\, c_{pl})\{\, 1+a \pm [(1-a)^2 + (2c_{pl}/r\omega)^2]^{1/2}\}^{1/2}$$

where a is the ratio of Young's modulus to a factored shear modulus, E/fG (conveniently taken to be the square root of the ratio of longitudinal to Rayleigh wavespeeds), and r is the radius of gyration of the plate, $r = h/\sqrt{12}$ with h the thickness. This has two modes, one for the + and one for the - sign. At low frequencies, the + mode gives imaginary wavenumbers, so that these modes do not propagate. Above a certain cut-off frequency, however, the wavenumbers are real and a high speed propagation develops.

From this formula the wavespeed $c = \omega/k$ can be written as

$$c = \sqrt{2}c_{pl}/\{1+(c_{pl}/c_R)^2 \pm \{[1-(c_{pl}/c_R)^2]^2 + 4(c_{pl}/c_b)^4\}^{1/2}\}^{1/2}$$

where c_b is the bending speed $(Eh^3/12\mu)^{1/4}\, \omega^{1/2}$, where $\mu = \rho h$ is the plate areal mass density. The coefficient in this formula is equivalent to the vibrating beam stiffness coefficient (EI/μ). The dispersion formula thus has three parameters, c_{pl}, c_R (or their ratio, which depends only on Poisson's ratio), and h.

At low frequencies, the - mode reduces to $c = c_b$, which is 0 at 0 frequency, and at high frequencies to $c = c_R$. The + mode is usually of small magnitude and so is not considered further here, though should not be dismissed.

A graph showing the dispersive wavespeed for 3.2-mm (1/8-in) and 4.8-mm (3/16-in) thick aluminum plates is given in figure 4.4-1.

4.5 TRANSIENT MOTIONS

The motions controlled by these dispersion relations can be expressed by Fourier Integrals as superpositions of all frequency components. Thus, the response at the impact point can be written as

$$u(t) = \int U(\omega)\exp(i\omega t)d\omega,$$

where $U(\omega)$ is the transform of the motion, a complex variable, and can be written as

$$U(\omega) = A(\omega)\exp(i\phi_0(\omega))$$

A is the amplitude of each frequency component, and ϕ_0 is the phase. For an impulsive source, all components start as maxima at the same phase $\pi/2$. When these components propagate, each at a different speed, the signal is given by the Fourier Integral with shifted time $t' = t-x/c(\omega)$:

$$u(x,t) = \int U(\omega)\exp(i\omega(t-x/c))d\omega$$

so that the apparent phase of the transform of $u(x,t)$ is

$$\phi(\omega) = \pi/2 - \omega x/c(\omega)$$

Since the time of impact is not generally known, an unknown time-shift through t_0 occurs in the data, resulting in a spectral change. The measured waveform then has the spectral phase

$$\phi_m = \phi + \omega t_0 = \pi/2 - \omega x/c + \omega t_0$$

This formula shows that the phase spectrum contains the distance and time shift explicitly. Since the frequency dependence of the terms is known, it should be possible to use a regression analysis on measured spectra to obtain these. However, the phase varies as $\omega^{1/2}$ (since the speed c varies as $\omega^{1/2}$), and this leads to an infinite slope at zero frequency. Thus, the phase spectrum changes fast near zero. For a numerically-derived spectrum at discrete frequencies, the change between each point can be larger than 2π. Numerical analyses can only evaluate the principal phase, say between $-\pi$ and $+\pi$, so that uncertainty arises at the low frequency end of the spectrum.

4.6 DETERMINING LOCATION

Measurements of motion at several places provides data on travel time from the impact to several known places, with an unknown time shift common to all. Thus, for a known point (x,y) the travel time relative to an arbitrary time with the unknown shift t_0 is t. For a wave travelling with a speed c from the impact point (x_0,y_0), these are related by

$$r = \{(x-x_0)^2 + (y-y_0)^2\}^{1/2} = c(t+t_0)$$

Any error in this determination can be written as

$$e = r - c(t+t_0)$$

and a least squares definition of best fit defined as

$$\Sigma e^2 = \text{Min}$$

The variables in this minimization are the unknown impact position (x_0, y_0) and the time shift t_0. The minimization leads, by differentiation, to the equations

$$\Sigma e(de/dx_0) = \Sigma e(de/dy_0) = \Sigma e(de/dt_0) = 0$$

which can be written as the following implicit equations

$$x_0 = \{\Sigma ex/r\}/\{\Sigma e/r\}$$

$$y_0 = \{\Sigma ey/r\}/\{\Sigma e/r\}$$

$$t_0 = \Sigma r/c - \Sigma t$$

An iteration scheme based on these equations serves to determine x_0, y_0, and t_0 from several waveforms.

4.7 DATA INTERPRETATION

The main task is to determine the distance of the impact by using data from the measured waveforms. Assuming simple wave propagation, the time of travel of the waves and their known wavespeed gives this distance except for the unknown time origin.

To estimate wave travel time, the onset of motion (first break in the signal) is determined by assigning a threshold. The practical problem is to distinguish between signal, noise, and late arrivals, since the first motion is small and larger motions represent modes at varying wavespeeds. The fastest waves are the in-plane motions which decay rapidly with distance, followed by the high frequency Rayleigh waves. Trailing these at ever lower speeds are the bending waves, which can be the largest. To evaluate this problem, the first break has been determined for several thresholds as discussed in Results. Using the Fourier transform phase spectrum as an alternative means of determining distance has been evaluated and is also discussed.

5.0 RESULTS

The recorded waveforms have been analyzed in four ways as follows: 1) the accuracy of defining time-of-arrival for first-break of motion in the signals; 2) position estimates by the error minimizing method from several waveforms; 3) the Fourier transform method; and 4) feature analysis as a prelude to pattern recognition.

5.1 FIRST BREAK ANALYSIS

A typical waveform (from the sensor at 254-mm (10-in) from file IMP2.DAT of 1/21) is shown, together with early details on enlarged time scales, in figure 5.1-1. The earliest pulse train, amplified at the lower left of the figure, appears to have a slight inverse dispersion, with frequency decreasing along the pulse. The large later pulse train shown at the lower right is strongly dispersive with the frequency increasing steadily by a factor of ten or so after about 0.3 milliseconds. (The clipping of this waveform does not affect these features, which are also displayed by other waveforms, but inclusion of this trace was preempted by early data reduction.) This behavior, which represents slower propagation as frequency decreases, is characteristic of bending motions.

Similar details of four different waveforms all at one distance (sensors 1 to 4 from 0325_1.AE) are shown in figure 5.1-2, displaying measurement repeatability to within a few microseconds. For wavespeeds up to 6 mm/microsecond, however, this represents errors of up to 20 mm.

All waveforms for which signals were recorded from two sensors in line with the impact have been analyzed for arrival time using a sequence of thresholds. The baseline of the recordings for the first 100 points was first found, and then data were shifted to this baseline and smoothed by forming moving averages over 7 points. The time of first occurrence of a signal above each of five levels in a doubling sequence of thresholds were then found. The difference in distance and times for the pairs of waveforms are given in figure 5.1-3. Data for the six tests of 0325_1 and _2

21
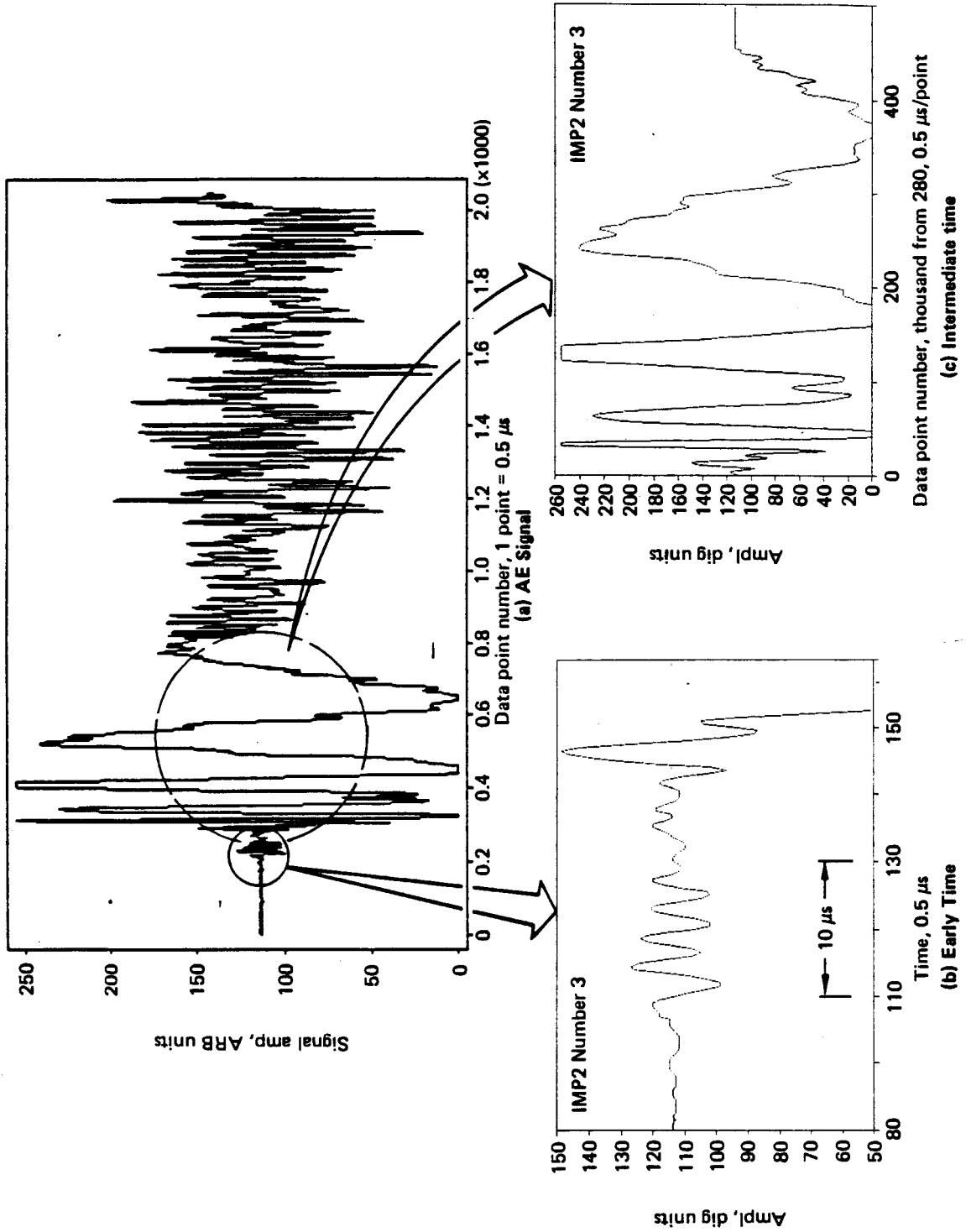
Figure 5.1-1. Details of One Trace
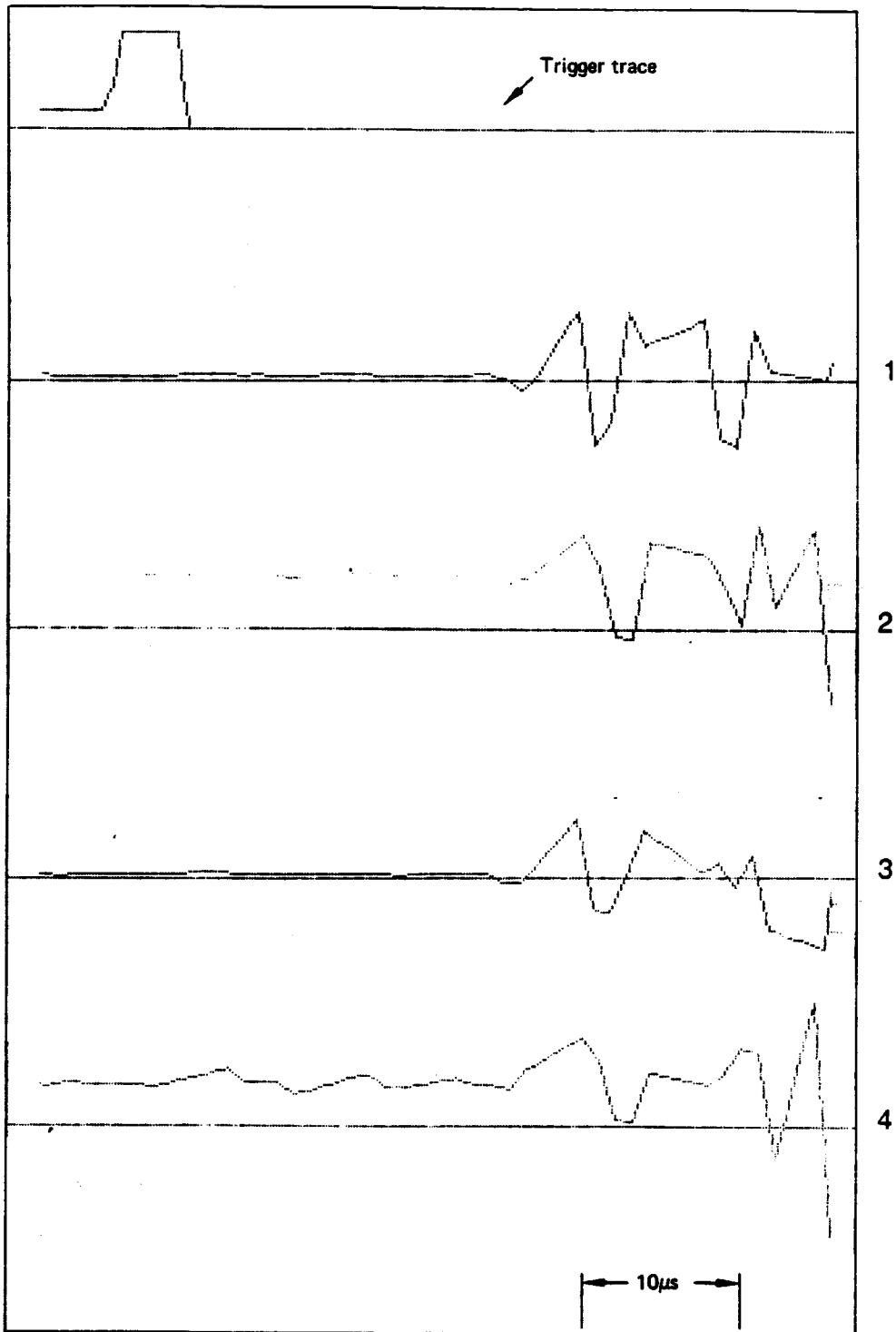
Figure 5.1-2. Comparison of Early Time Data in Tests of 03/25/87

Figure 5.1-3. Time-of-Arrival Data

File	Sensor Separation Distance (mm)	Avg Stddvn	Increment in TOA Between Sensors (microsec) Threshold (dig cts)				
			6	12	24	48	96
IMP1.DAT	160	0.28	26.5	18.5	16.5	45.5	44
IMP2.DAT	160	0.48	24.5	12	45.5	52	44
IMP3.DAT	287	0.33	12.9	24.6	28.5	55.8	
IMPACT.1	102	0.31	22.5	26	70	73	
IMPACT.2	102	0.1	32	35	32	76	
IMPACT.3	51	0.18	35.5	33.5	24.5	40	
IMPACT.4	51	0.13	33	27.5	28	42.5	
IMPACT.5	178	0.13	48	46.5	101		
IMPACT.6	178	0.1	36.5	45	98		
0306.1	178	0.09	32	34.5	40	93.5	
0306.2	102	0.31	2	5.5	19.5	72.5	
0306.3	51	0.09	5.5	6.5	6	18.5	

File	Sensor Separation Distance (mm)	Avg Stddvn	Threshold (volts)				
			1	2	4	8	16
0325_1.1	305	46	62	67	67	70	141
0325_1.2	305	46	68	69	78	115	119
0325_1.3	305	26	60	66	67	107	119
0325_1.4	305	90	5	8	65	105	114
0325_2.1	305	32	60	60	62	93	117
0325-2.2	305	23	63	106	107	106	103
0325_2.3	305	117	3	4	5	7	98
0325_2.4	305	36	59	59	63	108	106

(excluding the waveforms from sensor no. 4 which had low signals) are plotted against threshold level in figure 5.1-4. They show that for a threshold below about 5 volts the arrival time increment is between 60 and 65 microseconds, implying a wavespeed of 4.7 to 5.1 mm/microsecond, whereas above 7 volts, the times are between 105 and 120 for speeds of 2.5 to 2.9 mm/microsecond. A plot of the transit time data against distance for low and high thresholds from all tests is given in figure 5.1-5. The low threshold data are compared with a line representing the plate velocity of 5.7 mm/microsecond. The high threshold data are shown with a line at the Rayleigh velocity of 3.1 mm/microsecond. The scatter is large, though improves with distance.

5.2 POSITION LOCATION ESTIMATES

Using an iterative algorithm that minimizes the squared error in distance-time estimates, the time-of-arrival data of 04/06 and 04/07 have been analyzed to find impact positions. The results are plotted in figure 5.2-1. Accuracy of location is within about 75-mm (3-in).

5.3 FOURIER SPECTRAL ANALYSIS

Spectral analysis was made by two methods: the simple zero-crossings technique and the Fast Fourier Transform (FFT) technique. The magnitude and cumulative phase spectra derived from an FFT of the waveform of IMP2 are shown in figure 5.3-1. The uncertainty in phase at low frequency can be seen. For this test where the distance is known, the wavespeed was calculated from the phase, with a shift to ensure a parabolic fit near zero, and plotted as a function of frequency in figure 5.3-2. The wavespeed characteristic for transient bending in a plate, discussed above, was also calculated for the known position of the sensor and superimposed on the measurement in figure 5.3.2. The agreement is good.

5.4 FEATURE ANALYSIS

A software package for extracting features from waveform data, the 4060 System (reference 4) developed by General Research Corp for their ALN 4060 Flaw Discriminator, was used on three of the waveforms from different distances in tests of 2/10 (the IMPACT.DAT file).

D180-30550-3
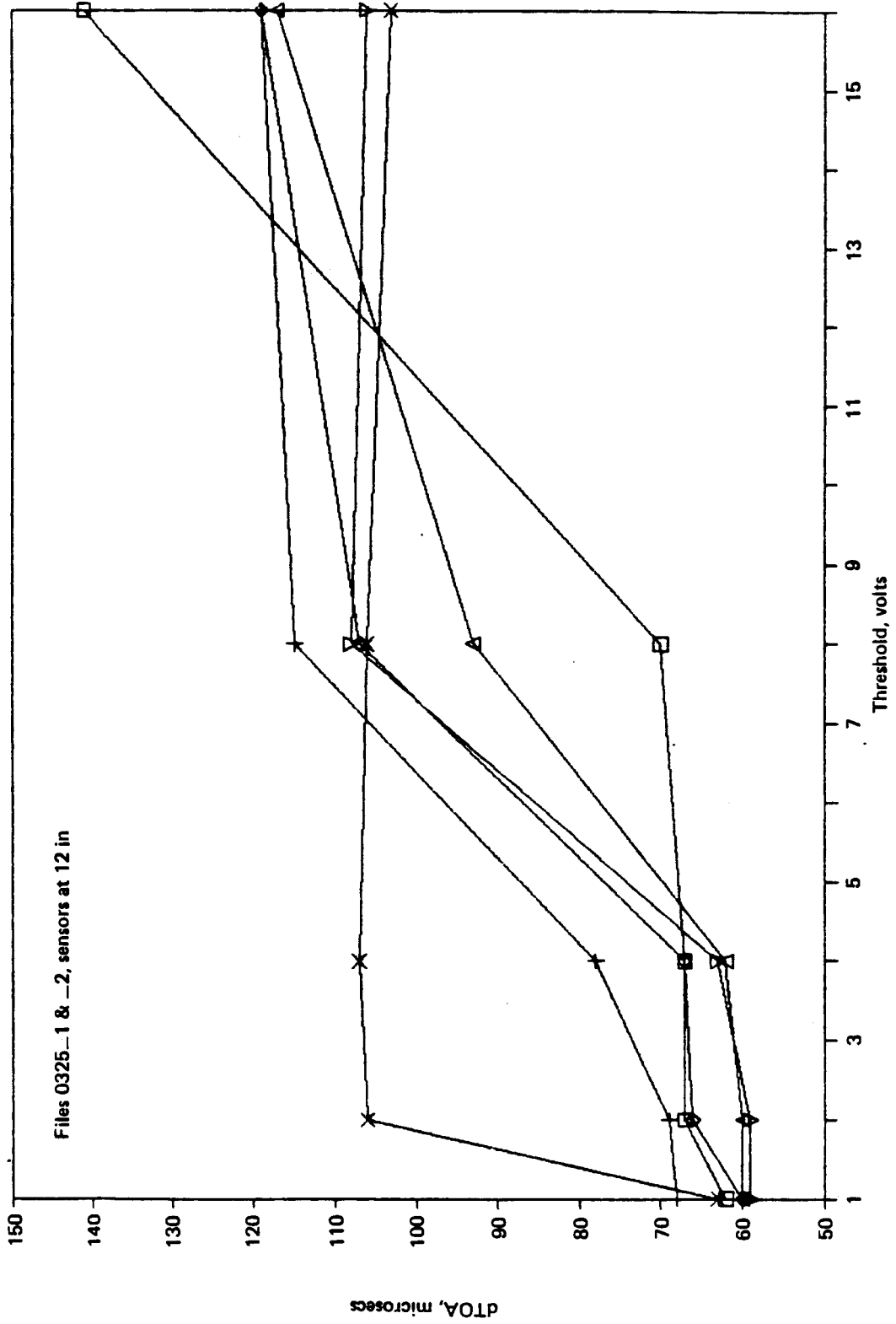
Figure 5.1-4. Differential Time-of-Arrival Data

26
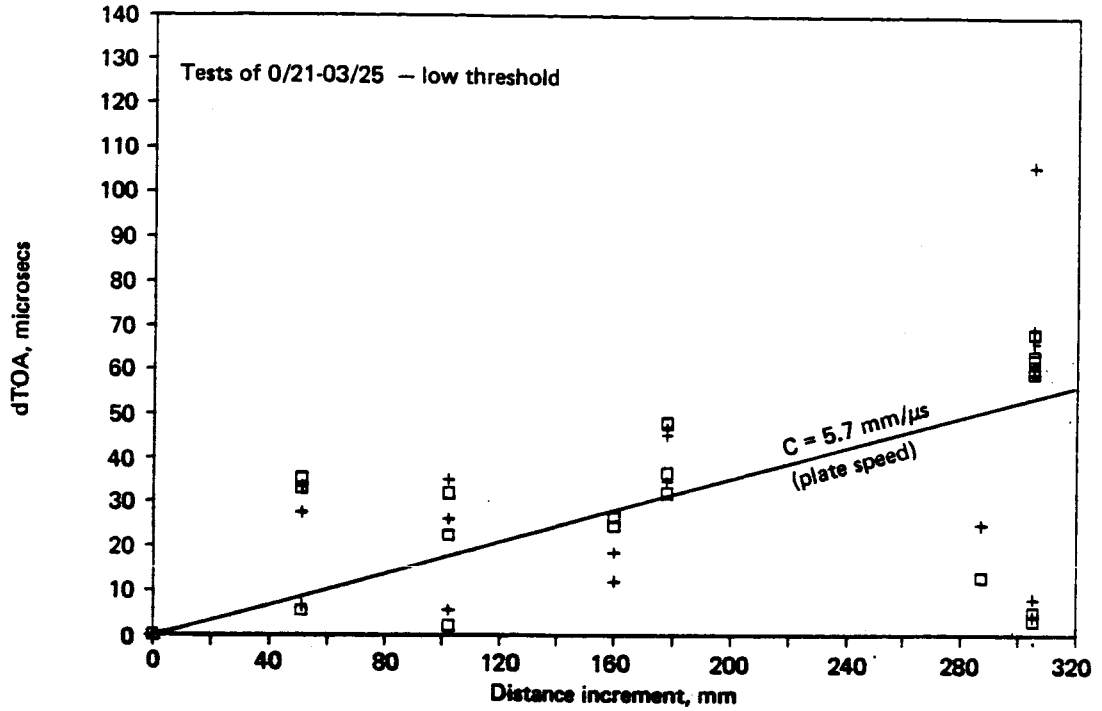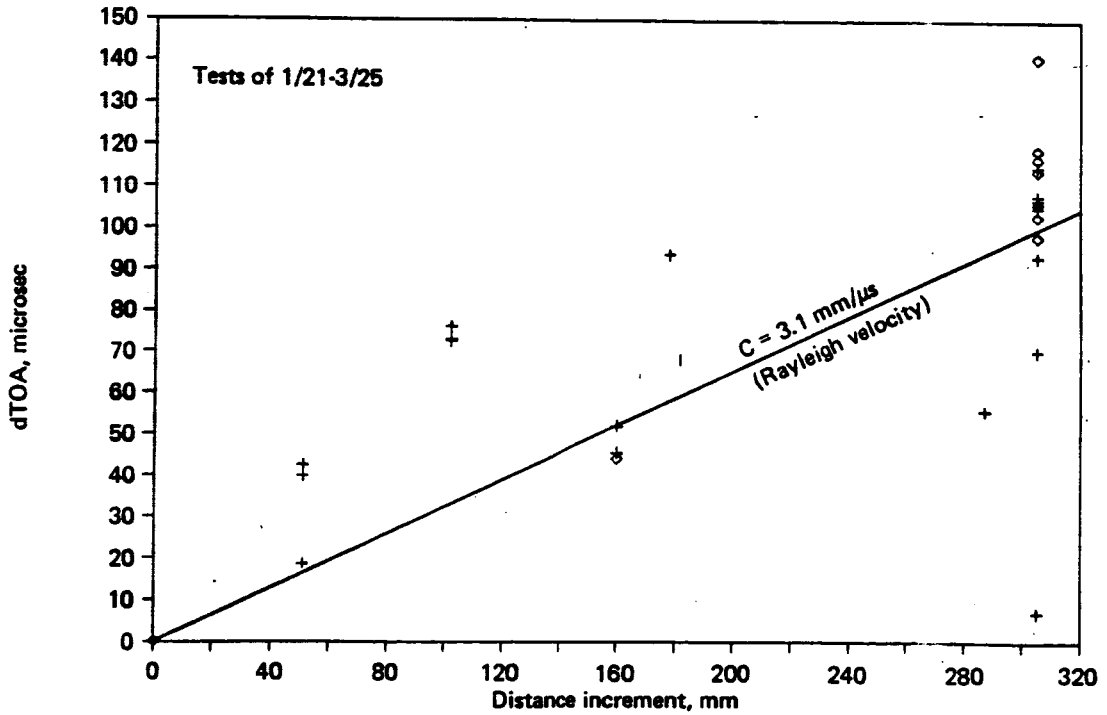
Figure 5.1-5. Incremental Time-of-Arrival Data Plotted for Distance Propagated
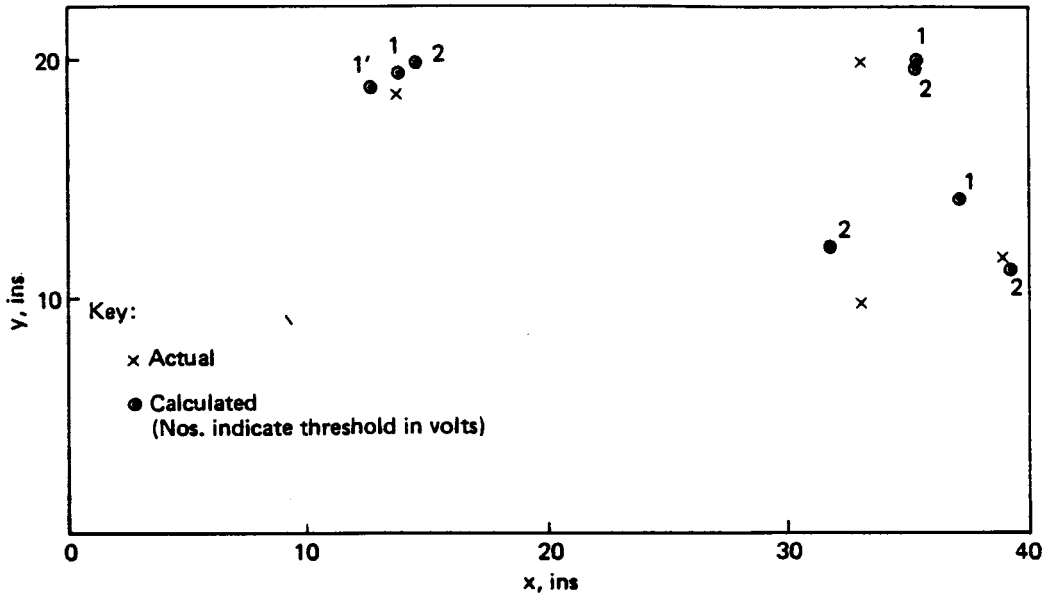
Figure 5.2-1. Comparison of Calculated and Actual Impact Positions
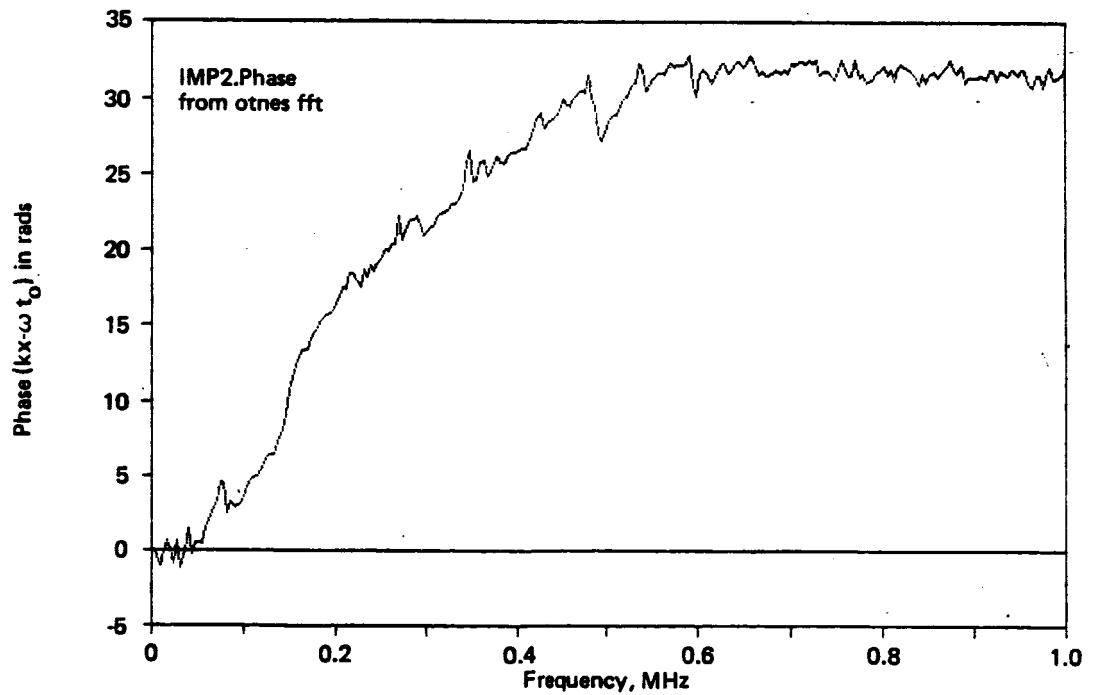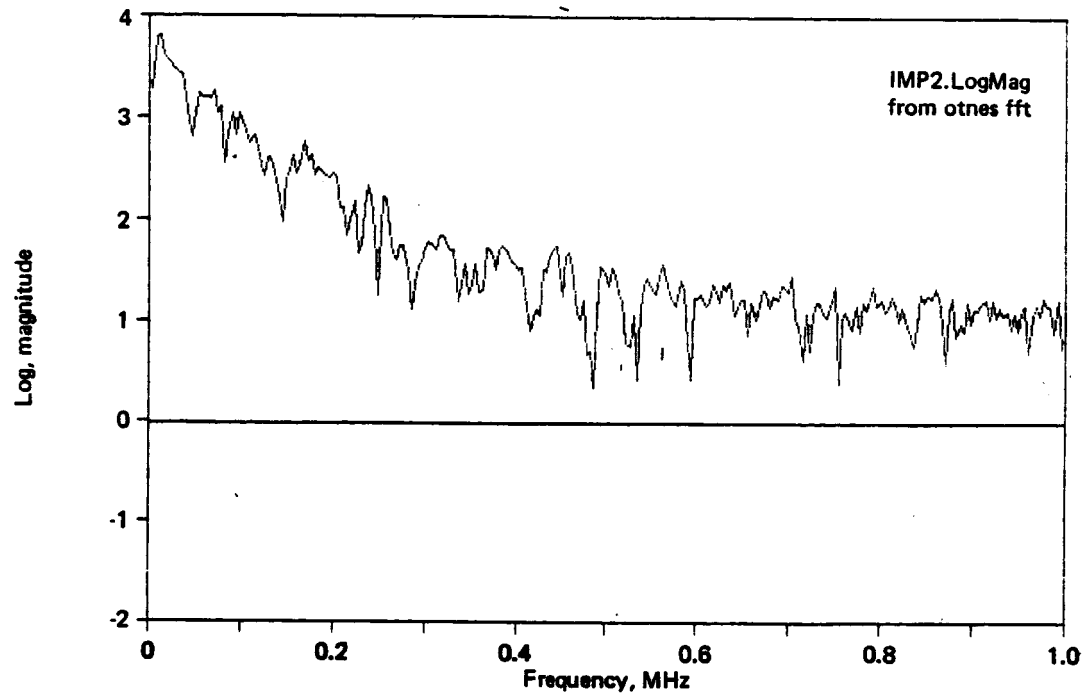
Figure 5.3-1. Magnitude and Phase Spectra of Bending Pulse
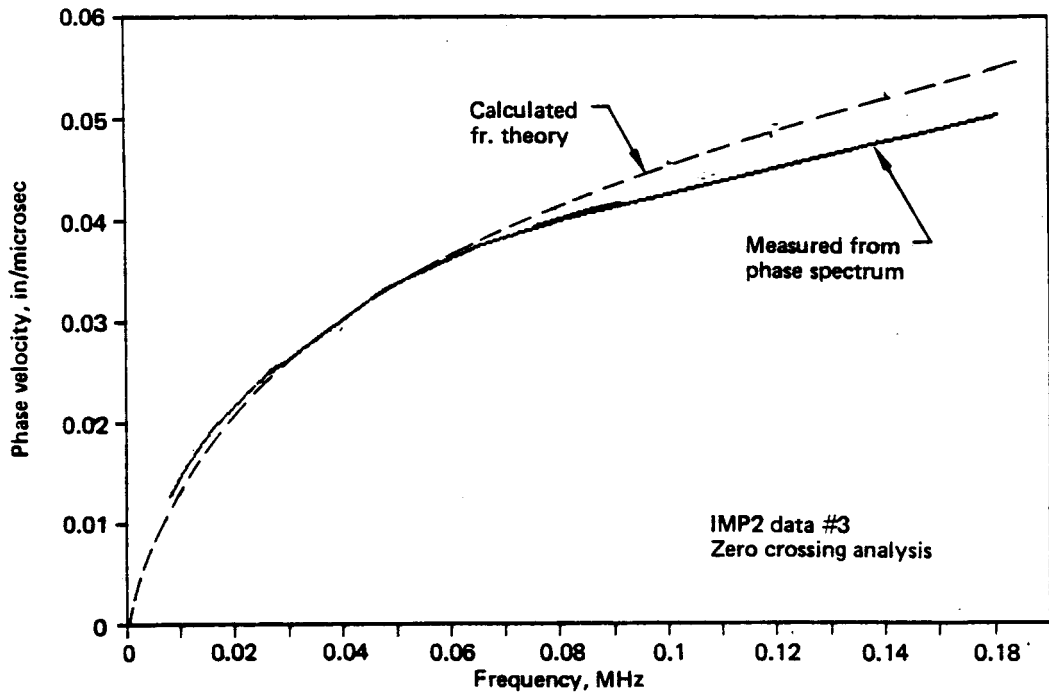
Figure 5.3-2. Comparison of Measured and Predicted Wavespeed

The software produces numerical values of 89 quantities such as peak amplitudes, total energies, times between peaks, spectral maxima, and statistics of peaks. Some features such as times should be dependent on sensor position and some should not. Others should depend on impactor characteristics including speed or on plate response such as perforation. The features were reviewed briefly for correlation to sensor position, and six have been identified as plotted in figure 5.4-1. These are described as:

F1 - 25-90% rise time

F13 - Phase coherence

F14 - Phase coherence

F34 - Power in first 1/8 of power spectrum

F42 - Power in first 1/4 of power spectrum

F60 - Standard deviation of envelope
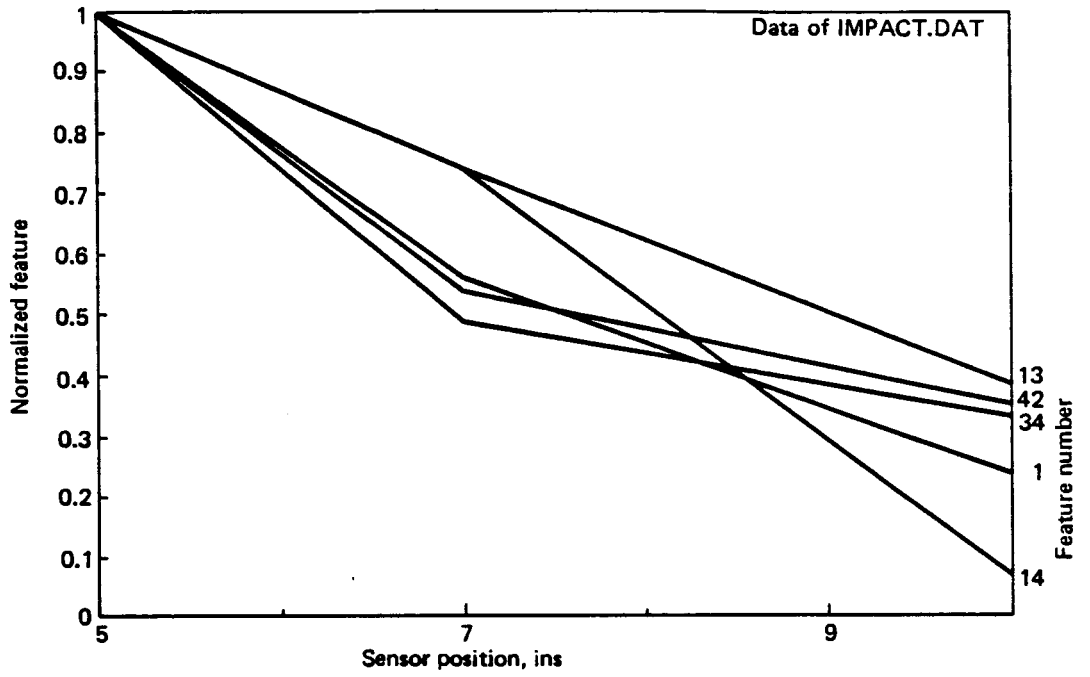
Figure 5.4-1. Correlating Features of Waveforms

6.0. CONCLUSIONS AND RECOMMENDATIONS

The test program and data analysis have provided some preliminary quantitative answers to the questions being addressed: the time resolution of the system used is about 3 to 5 microsecond, and this leads to a position accuracy of about 75-mm (3-in). Several types of sensors were tested and all were found to work satisfactorily. The most significant finding was that the Kynar thin-film piezoelectric material works, and this opens the opportunity to have many low-weight and low-cost sensors. Various data processing techniques have been found to be useful, but need further development for use in a practical system. A significant aspect of the problem needing further study is that of automatic scaling of data and automatic setting of thresholds of detection, when the impact characteristics are not known. Further work is recommended, both to analyze the existing data in more detail and to explore the effects of structural configuration on propagating waves.

REFERENCES

1. PEN 4 Version 8 Hypervelocity Impact Analysis, Boeing Aerospace Company, IR&D Doc. No. D180-29230-1, M. D. Bjorkman and J. D. Geiger, 27 February 1986.

2. Handbook of Engineering Mechanics, W. Flugge Editor, McGraw-Hill Book Company, 1962, p. 64-16, Vibrations/Propagation of Elastic Waves, by E. E. Zajac.

3. ibid, p. 61-14, Vibrations/Continuous Systems, by D. Young.

4. User's Guide and Technical Reference, 4060 Software System - Version 1.0, General Research Corp. December 1984.

Appendix A Waveforms for All Tests.
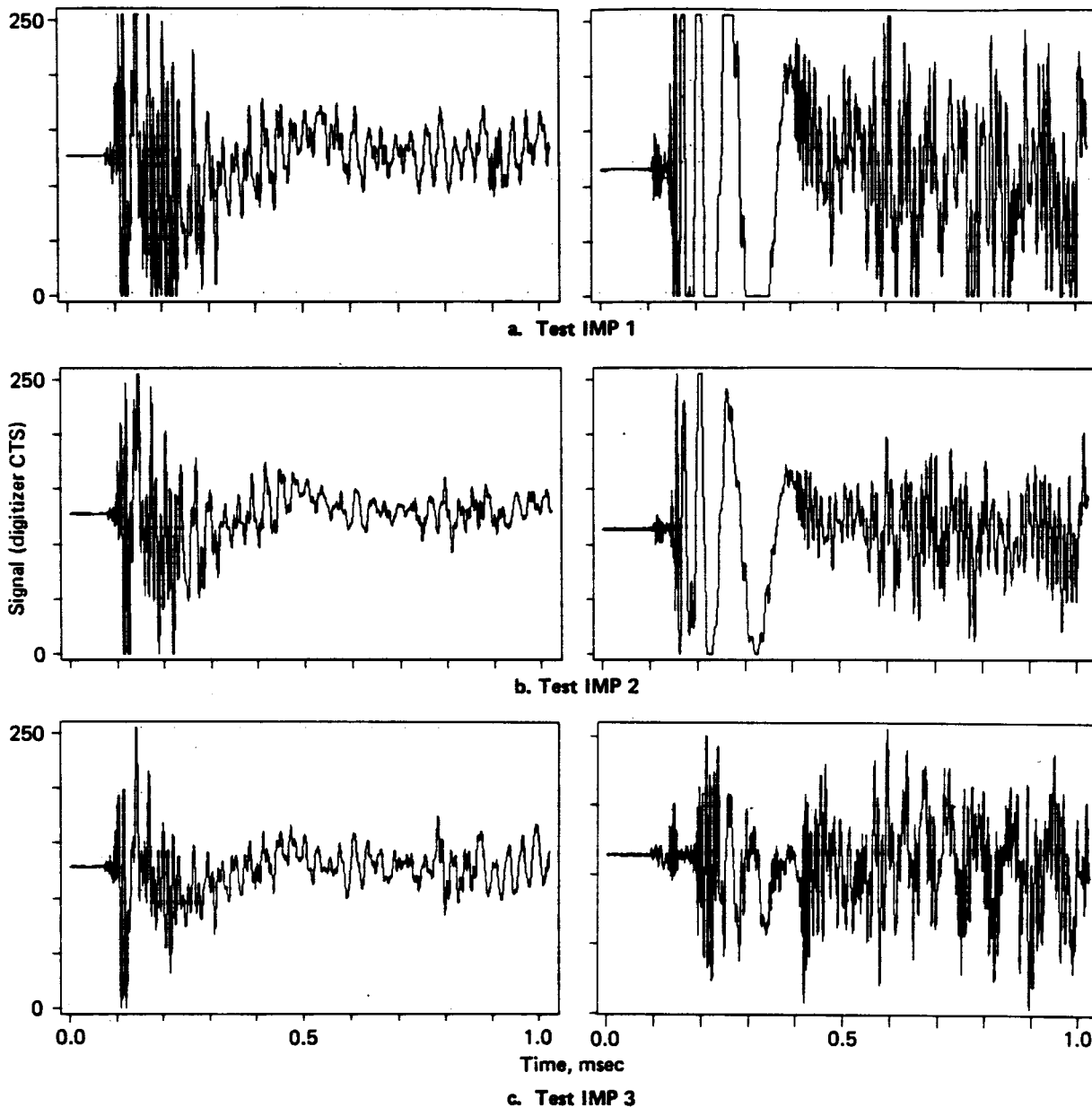
Figure A-1. Tests of 01/21/87: Three Repeats at 4 in and 10 in

a. Transducer at 5 in

b. Transducer at 7 in

c. Transducer at 10 in
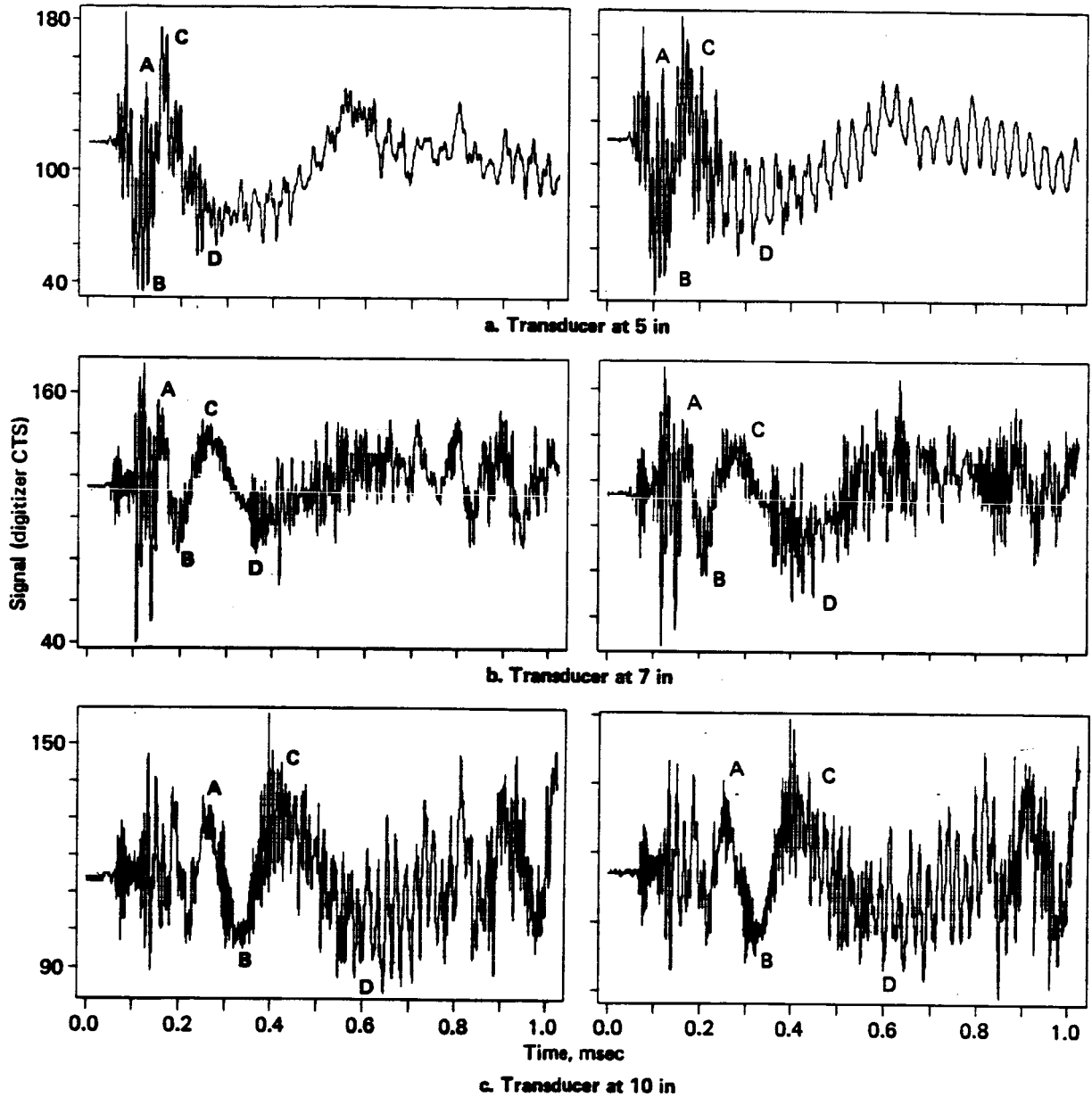
Note: A, B, C, and D denote four identifiable propagating peaks/troughs

Figure A-2. Tests of 02/10/87: Two Repeats at 5 in, 7 in, and 10 in
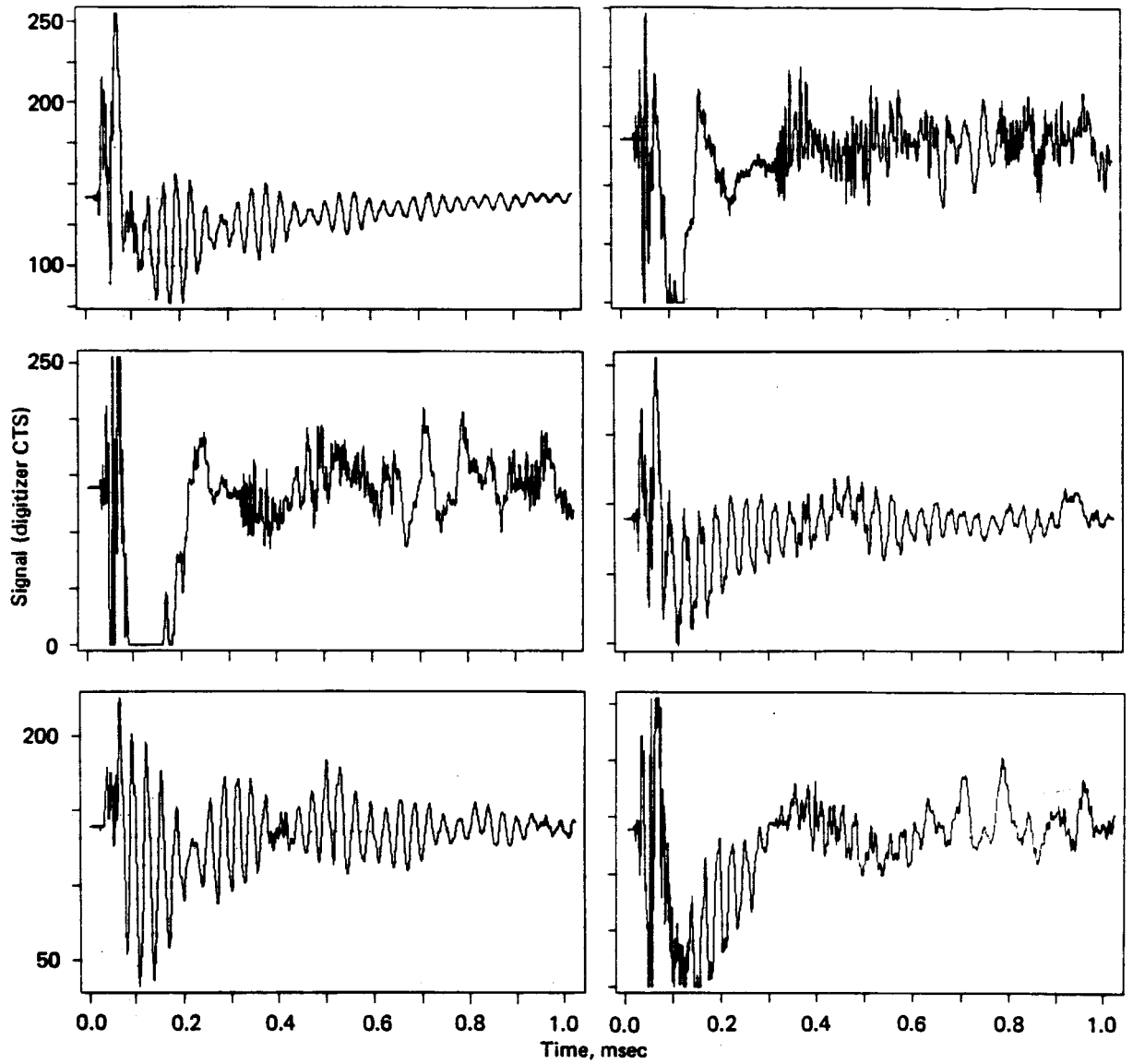
Figure A-3. Tests of 02/10/87: Six Repeats of Reference Transducer at 3 in
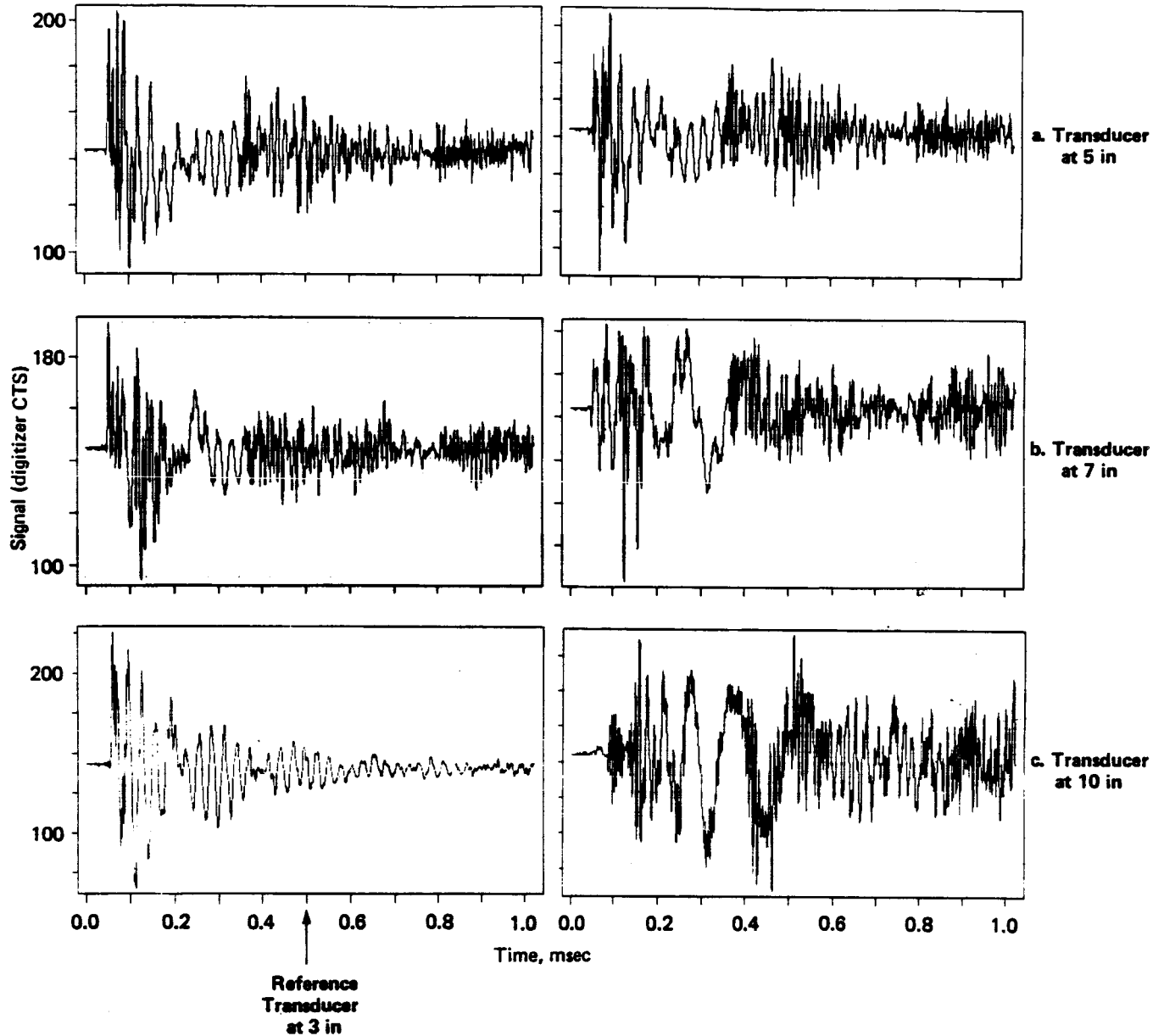
Figure A-4. Tests of 03/05, 06/87: Transducers at 5 in, 7 in, and 10 in Together With Reference at 3 in
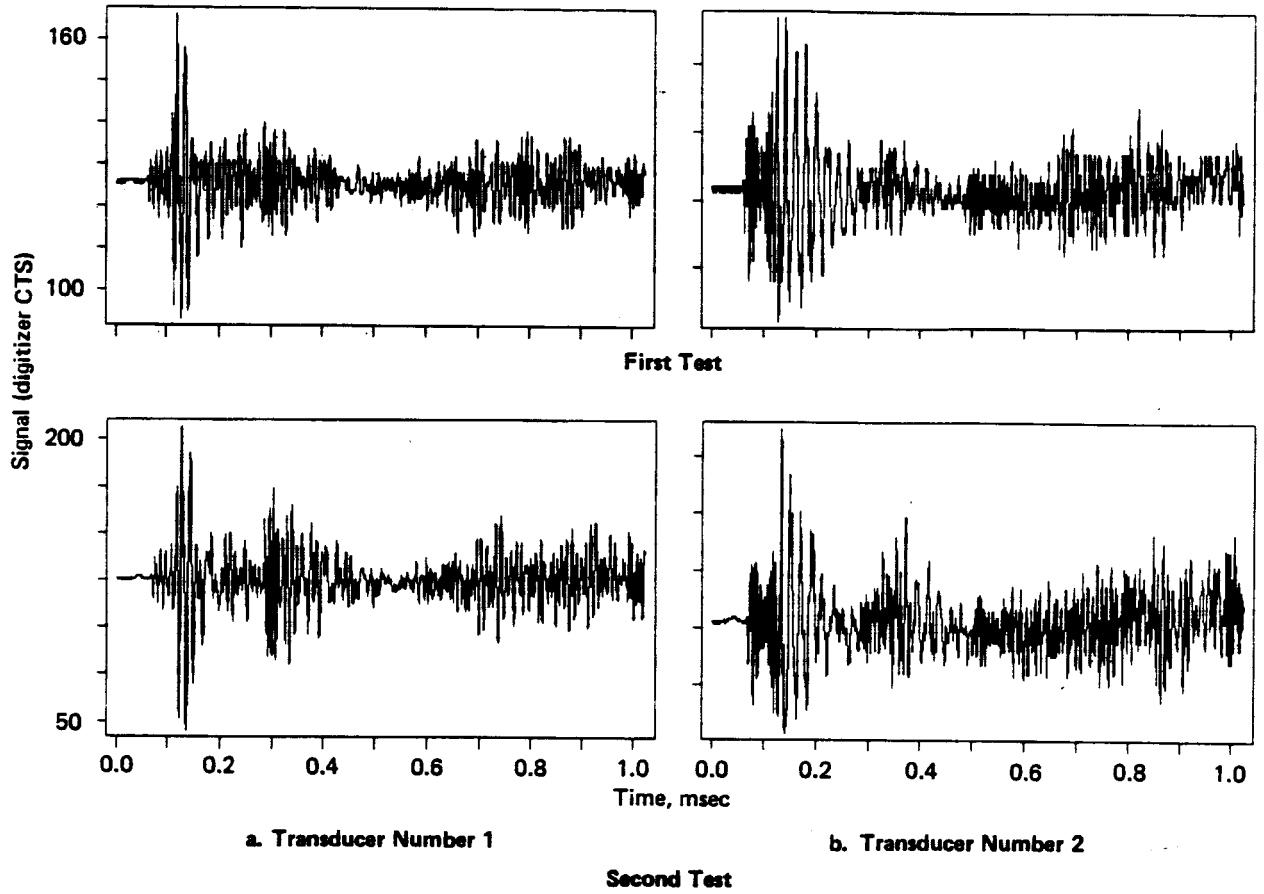
Figure A-5   Tests of 03/20/87: Two Repeats With Two Sensors at 10 in
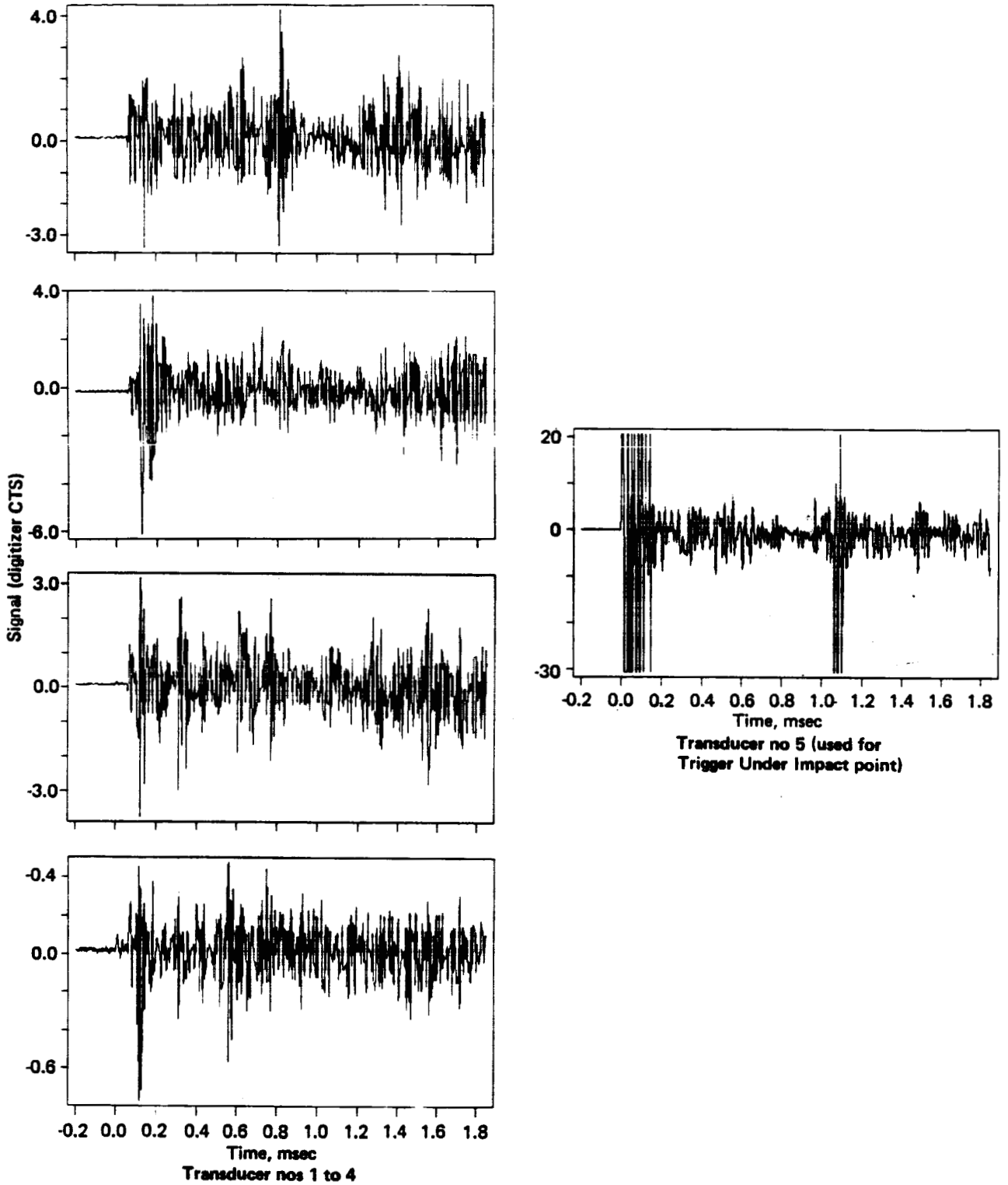
Figure A-6. First Test of 03/25/87: Four Transducers Close Together at 12 in and Trigger Transducer at 0 in

Trigger Under Imact

Four Transducers at 12 in
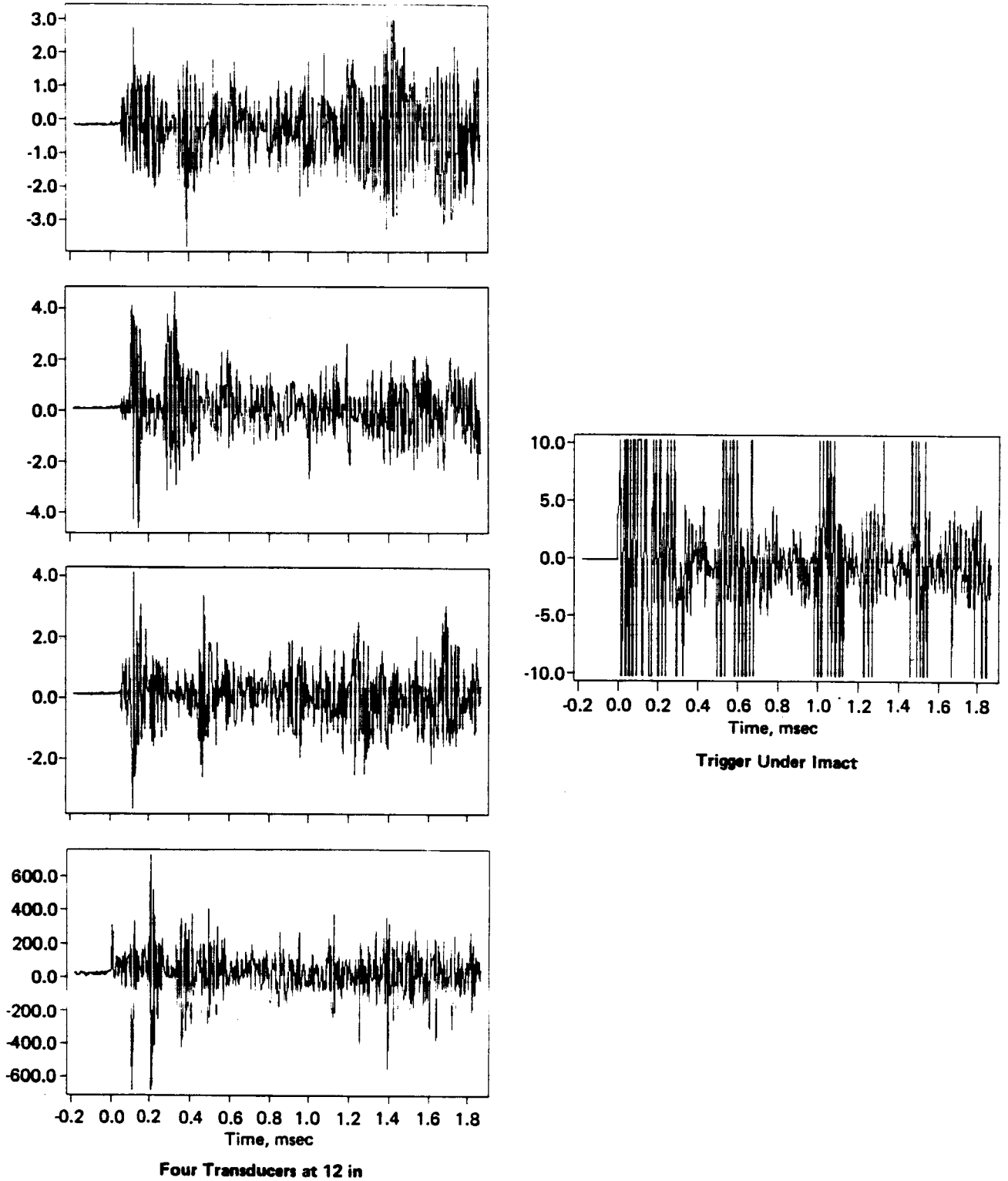
Figure A-7. Second Test of 03/25/87: Four Transducers at 45° Separations on 12 in Circle and Trigger Transducer at 0 in
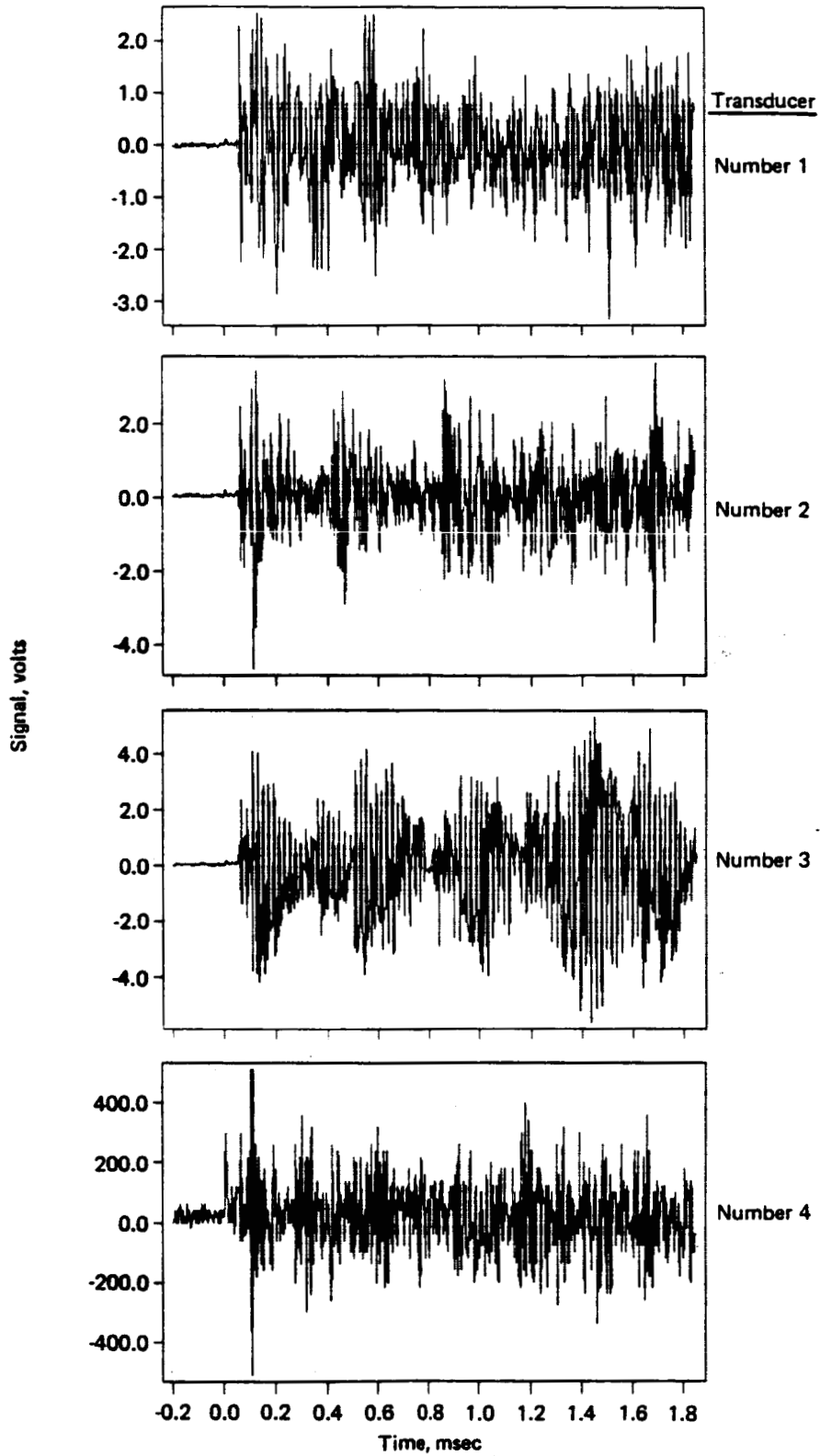
Figure A-8. Test of 04/01/87: Four Transducers at 45° Intervals on 12 in Radius

43
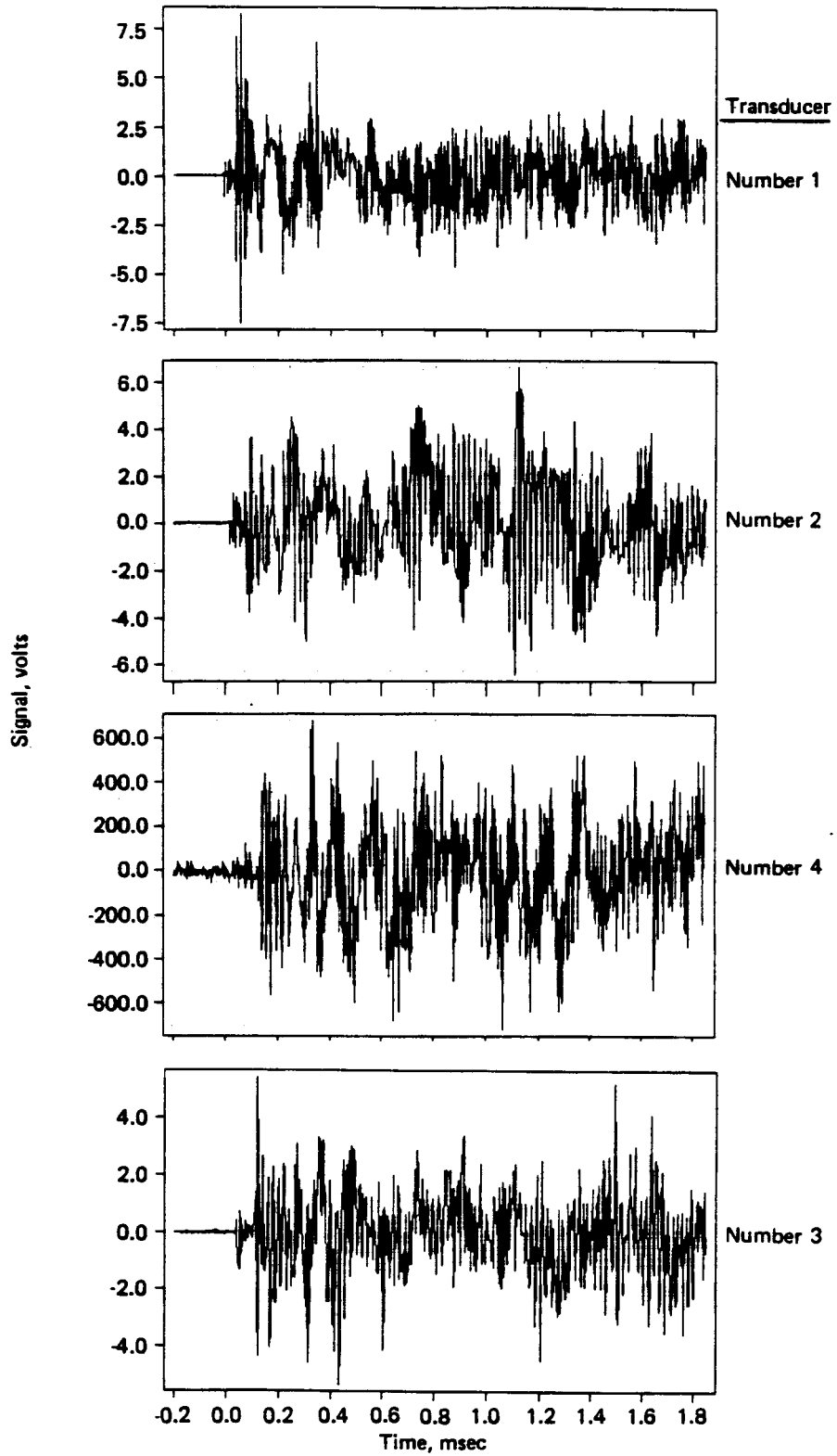
Figure A-9. Test of 04/02/87: Four Transducers at 45° Intervals on 12 in Radius

44
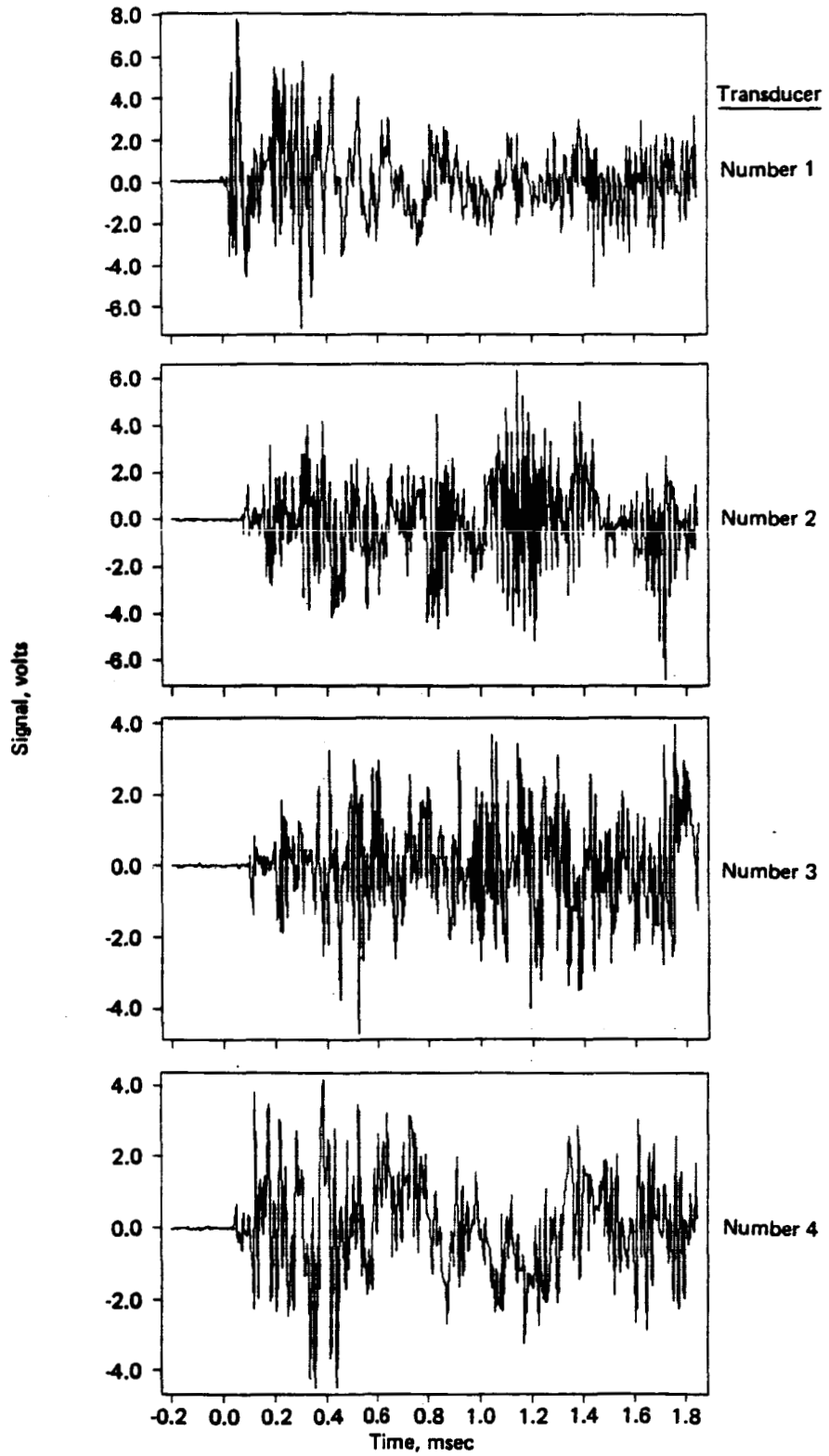
Figure A-10. First Test of 04/06/87: Four Transducers at 45° Intervals on 10 in Radius
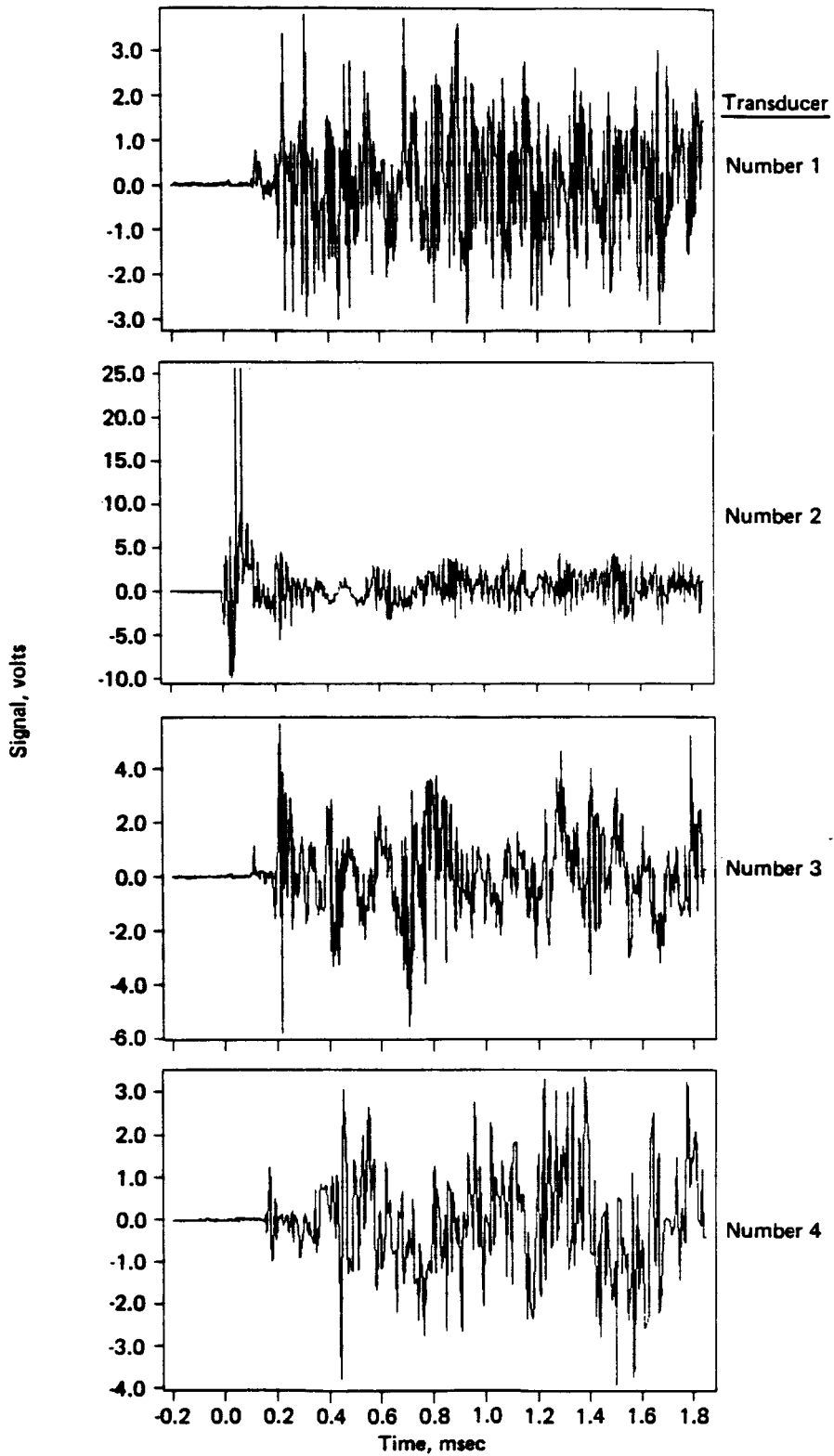
Figure A-11. Second Test of 04/06/87: Four Transducers at 45° Intervals on 10 in Radius

46
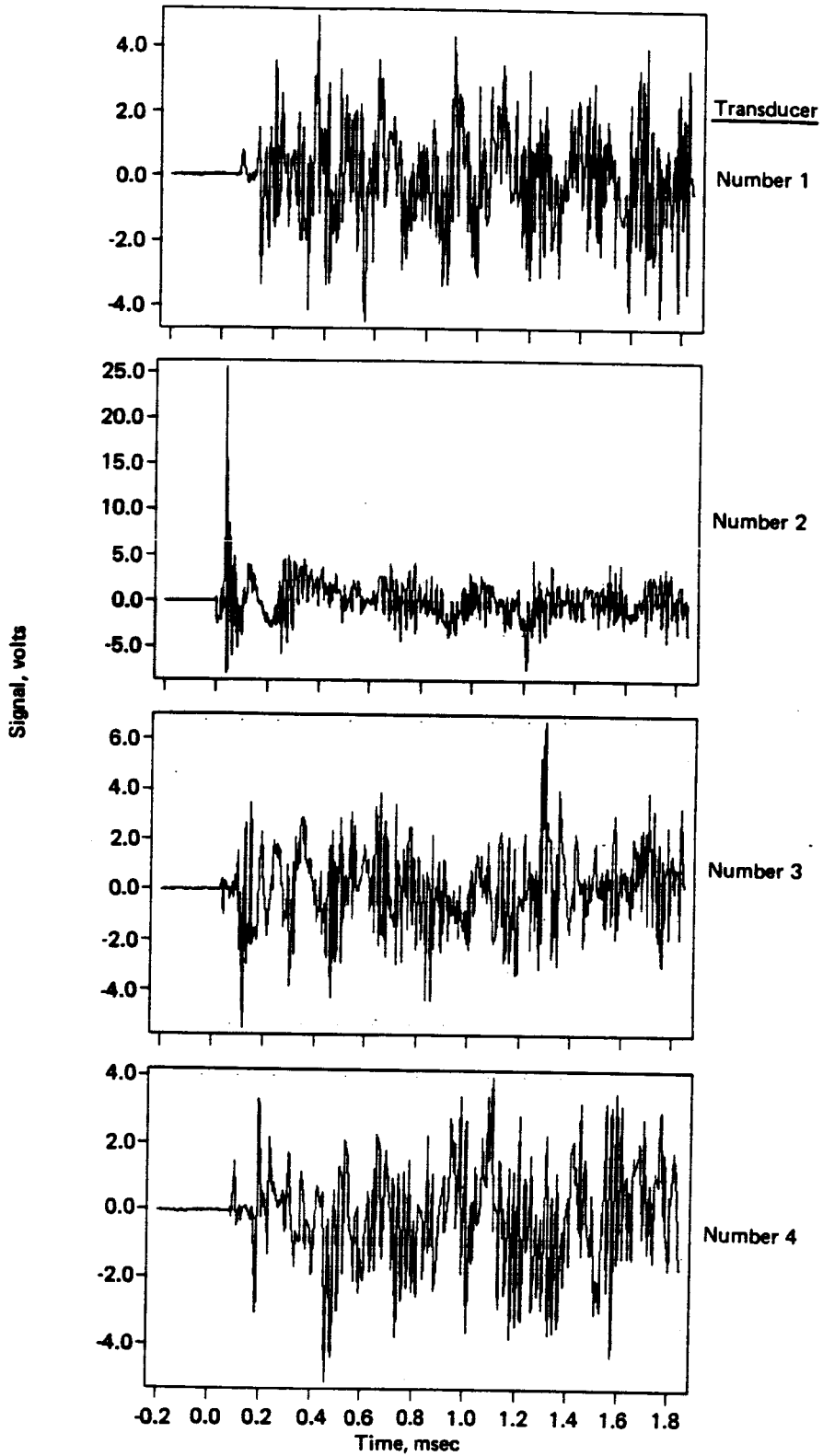
Figure A-12. Third Test of 04/06/87: Four Transducers at 45° Intervals on 10 in Radius
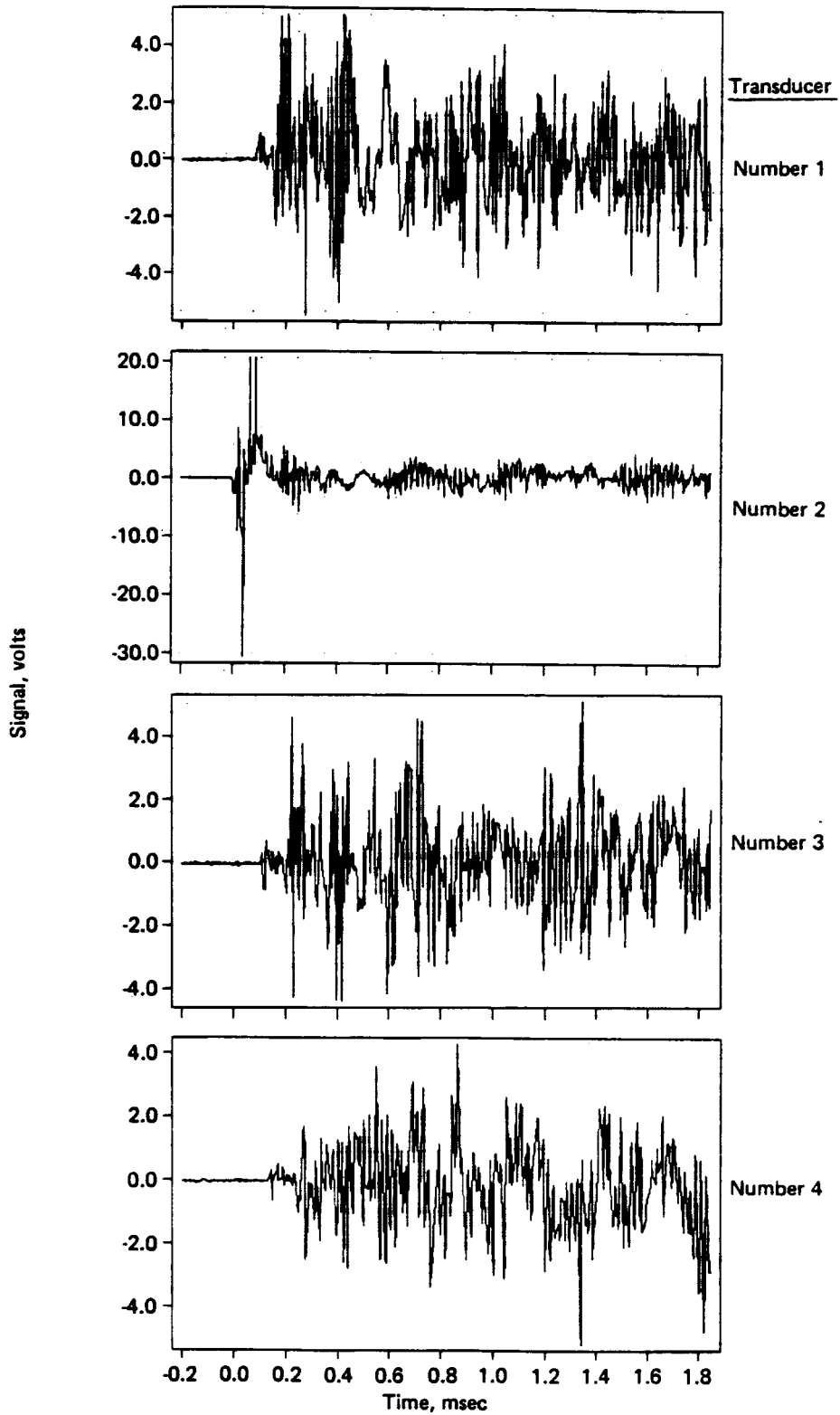
Figure A-13. Test of 04/07/87: Four Transducers at 45° Intervals on 10 in Radius
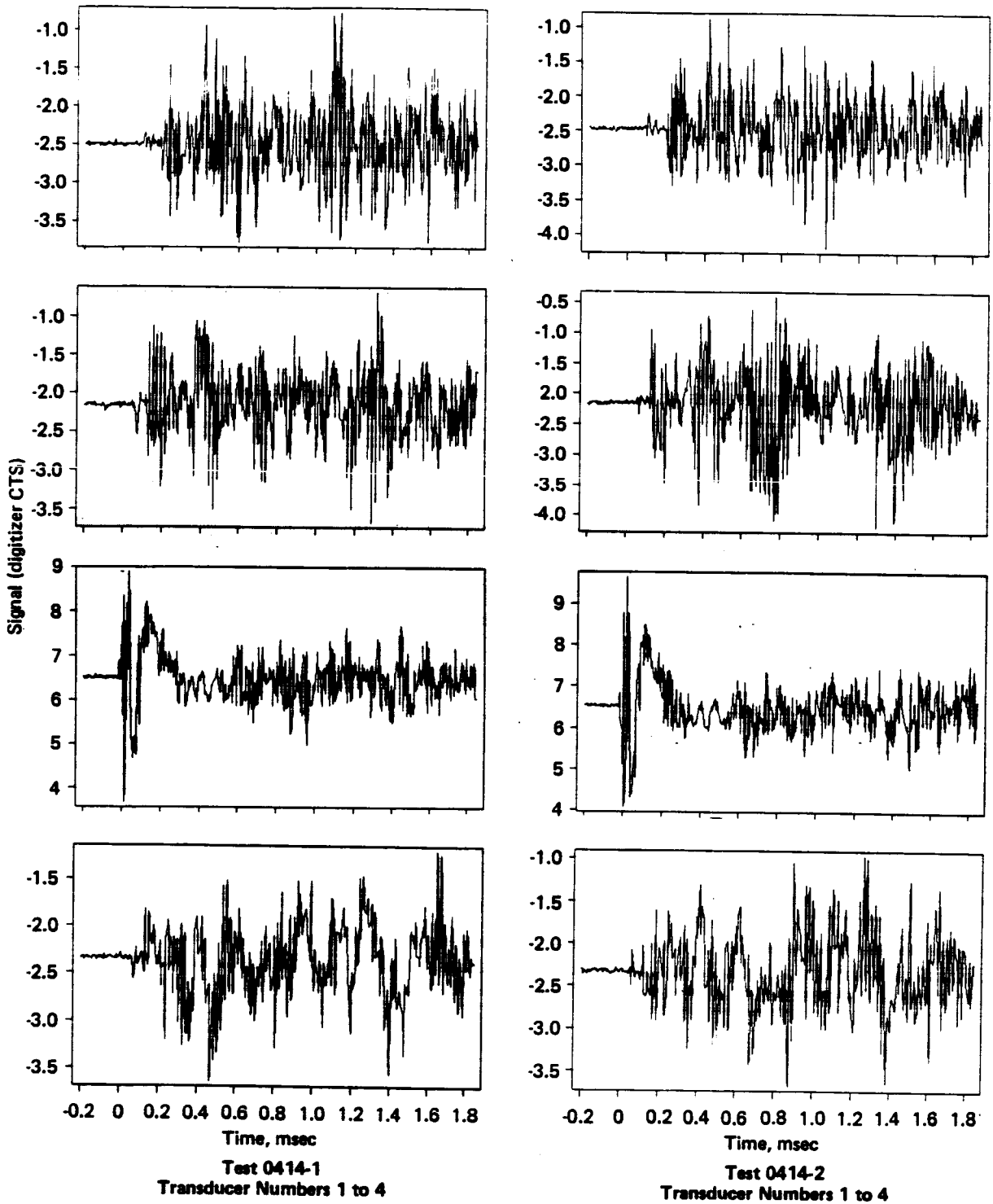
Figure A-14. First Two Test of 04/14/87.

49
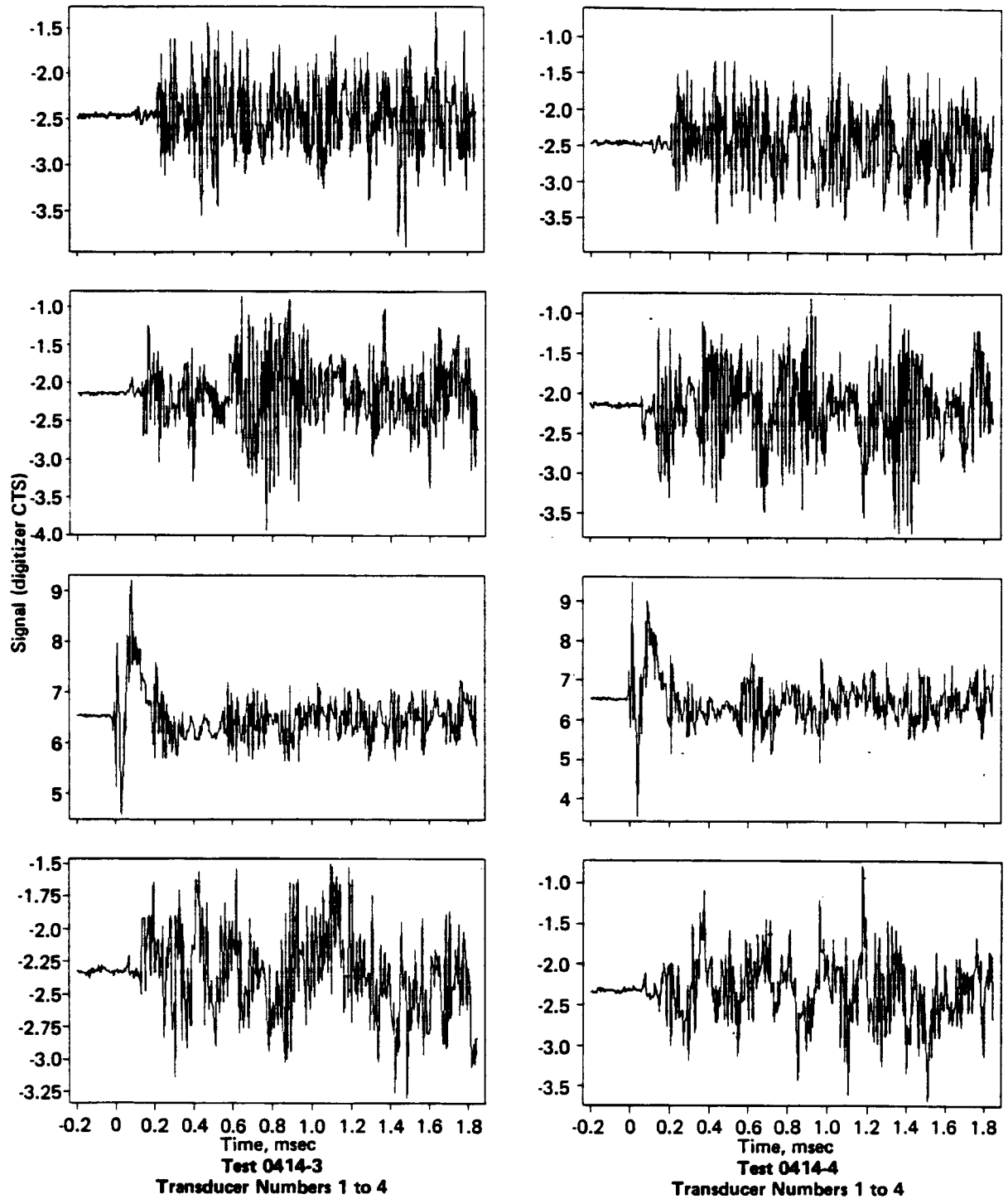
Figure A-15. Last Two Tests of 04/14/87
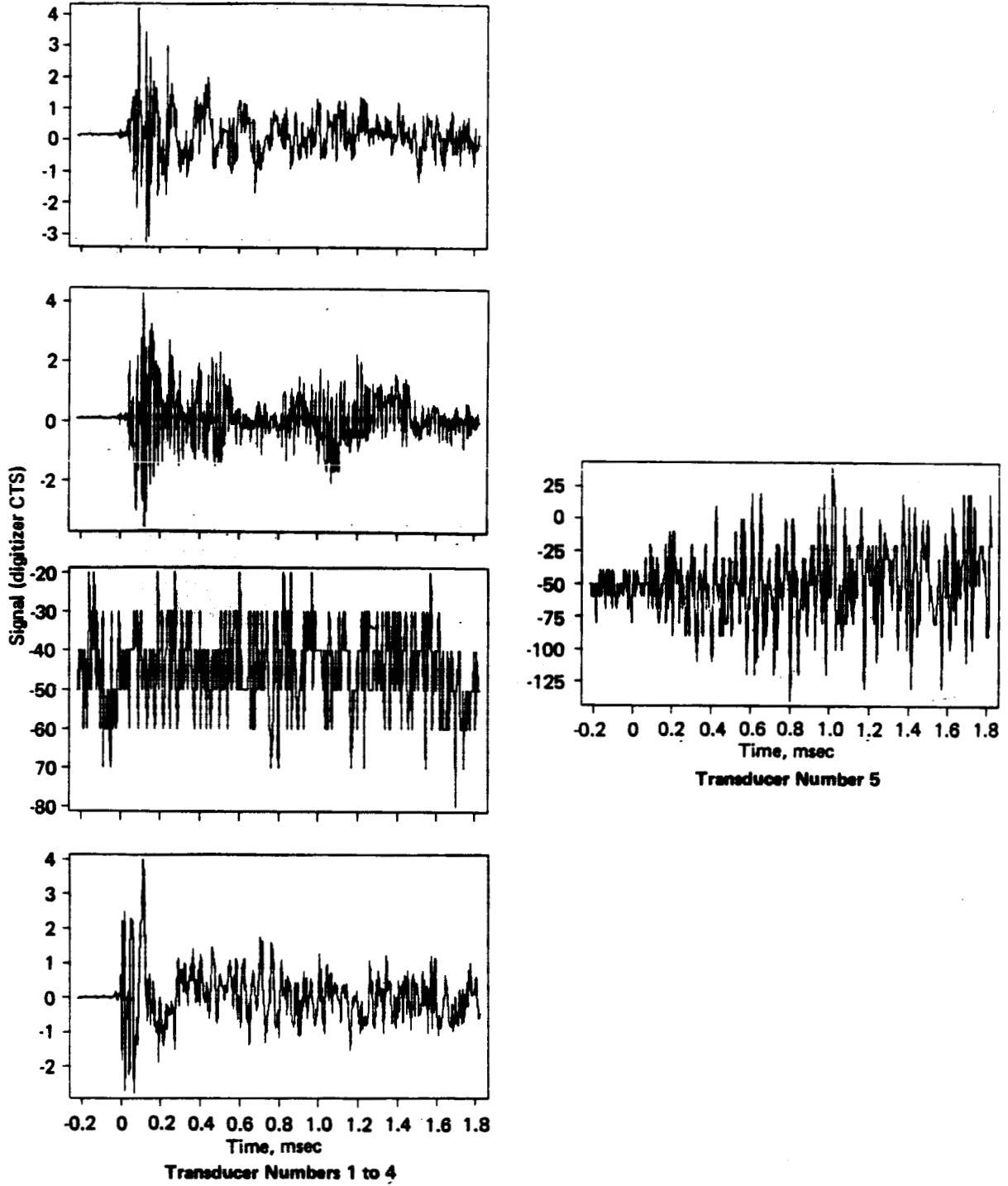
Figure A-16. First Test of 04/20/87

51
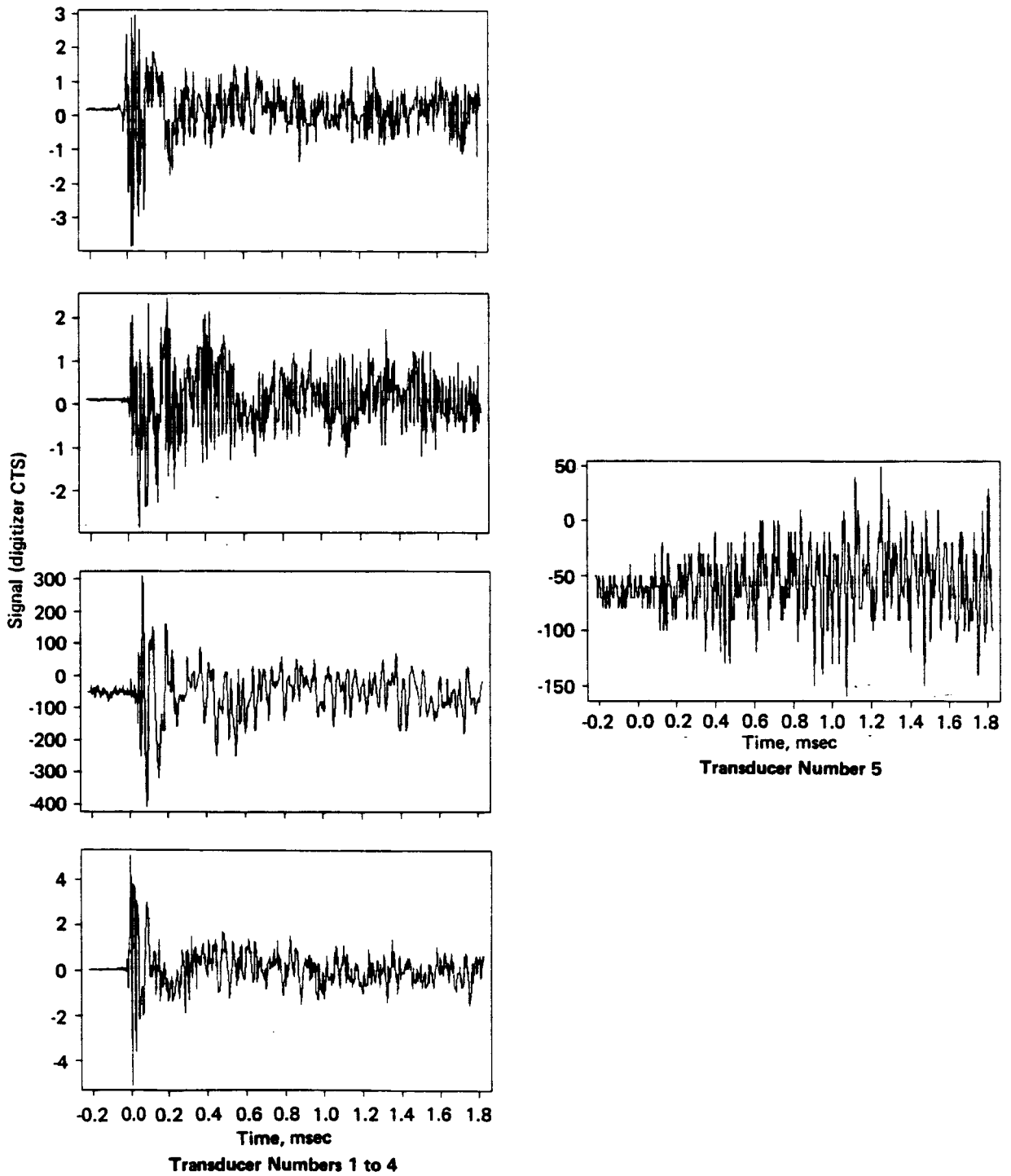
Figure A-17. Second Test of 04/20/87
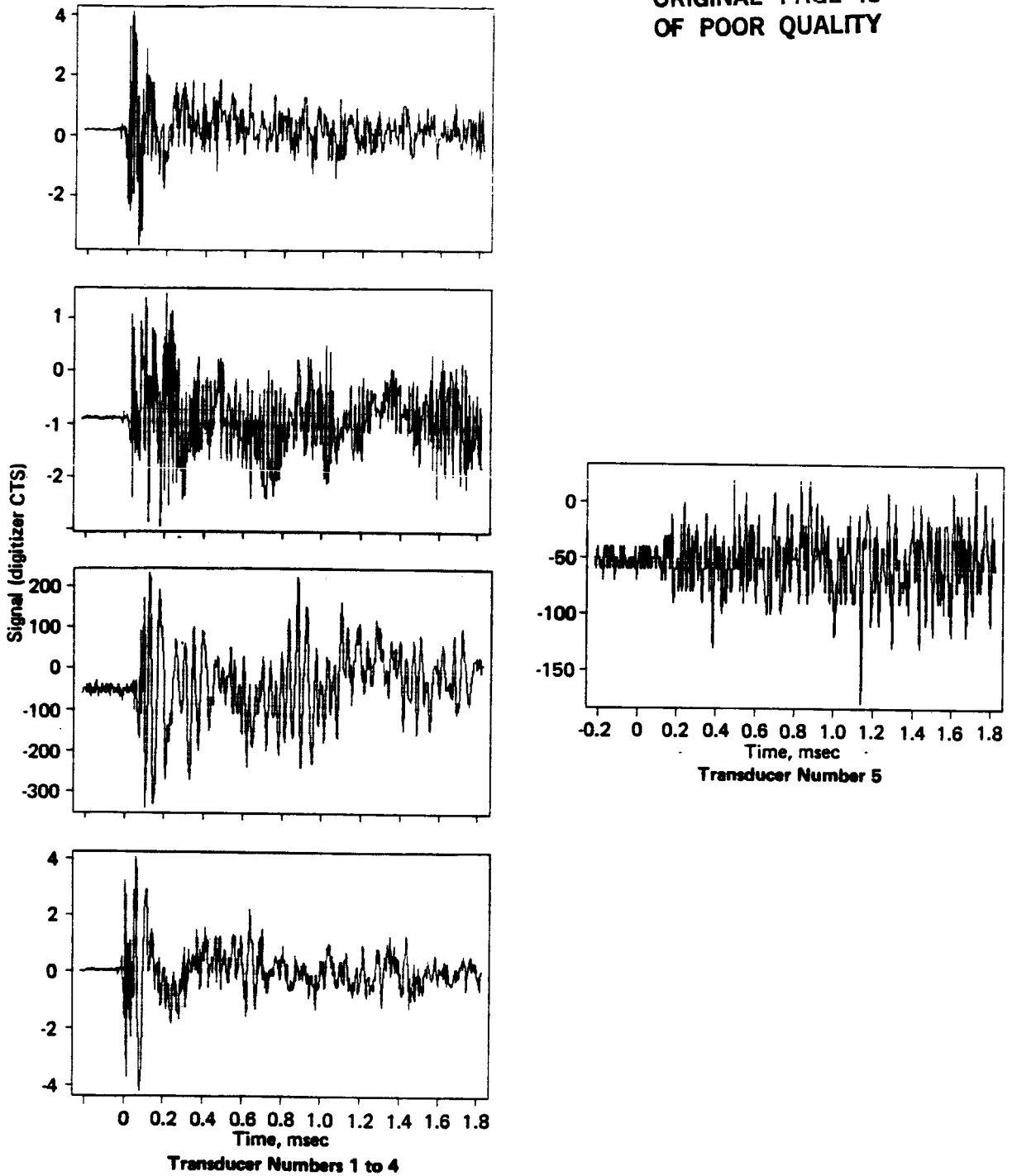
Figure A-18. Third Tests of 04/20/87
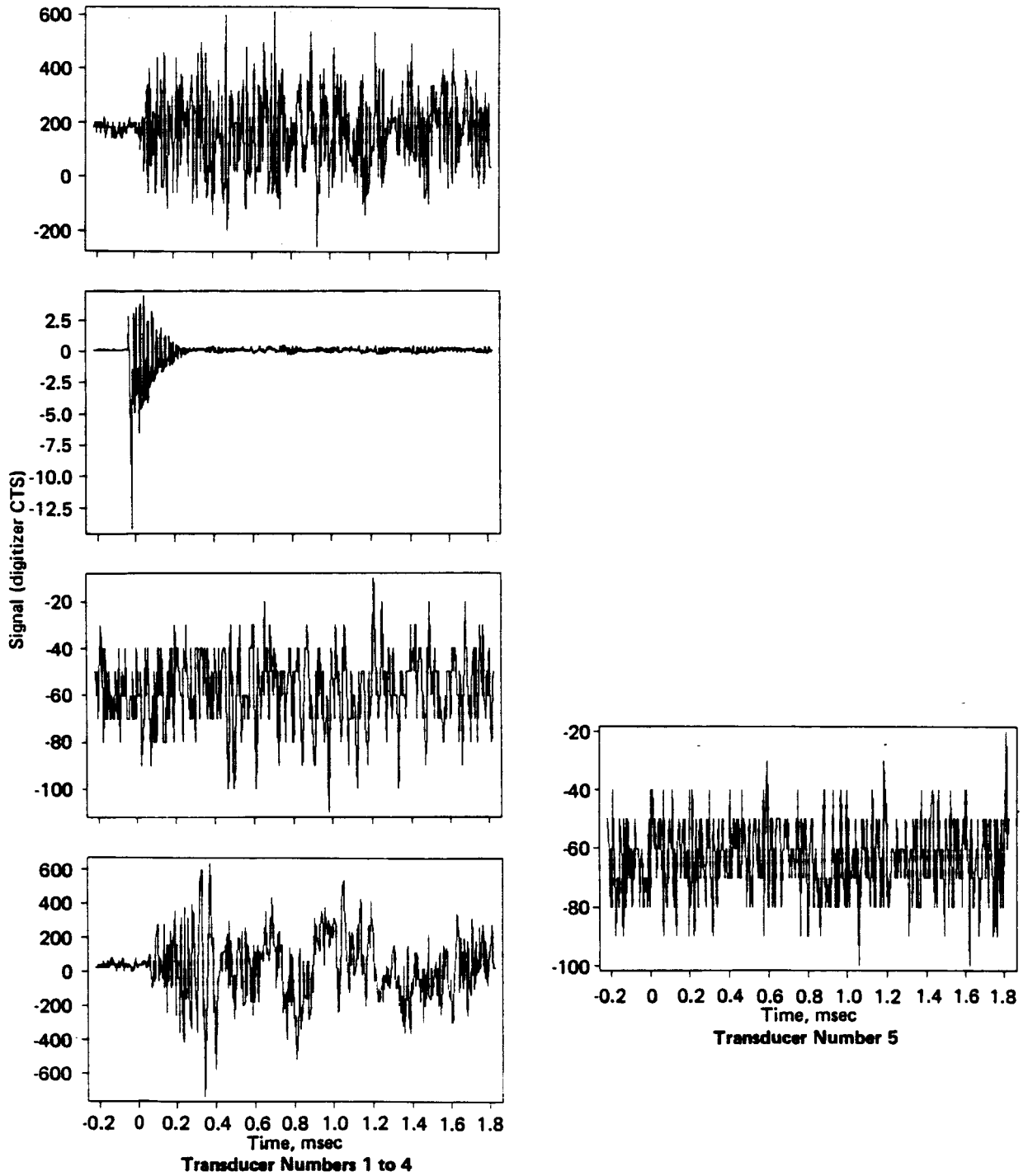
Figure A-19. Fourth Test of 04/20/87
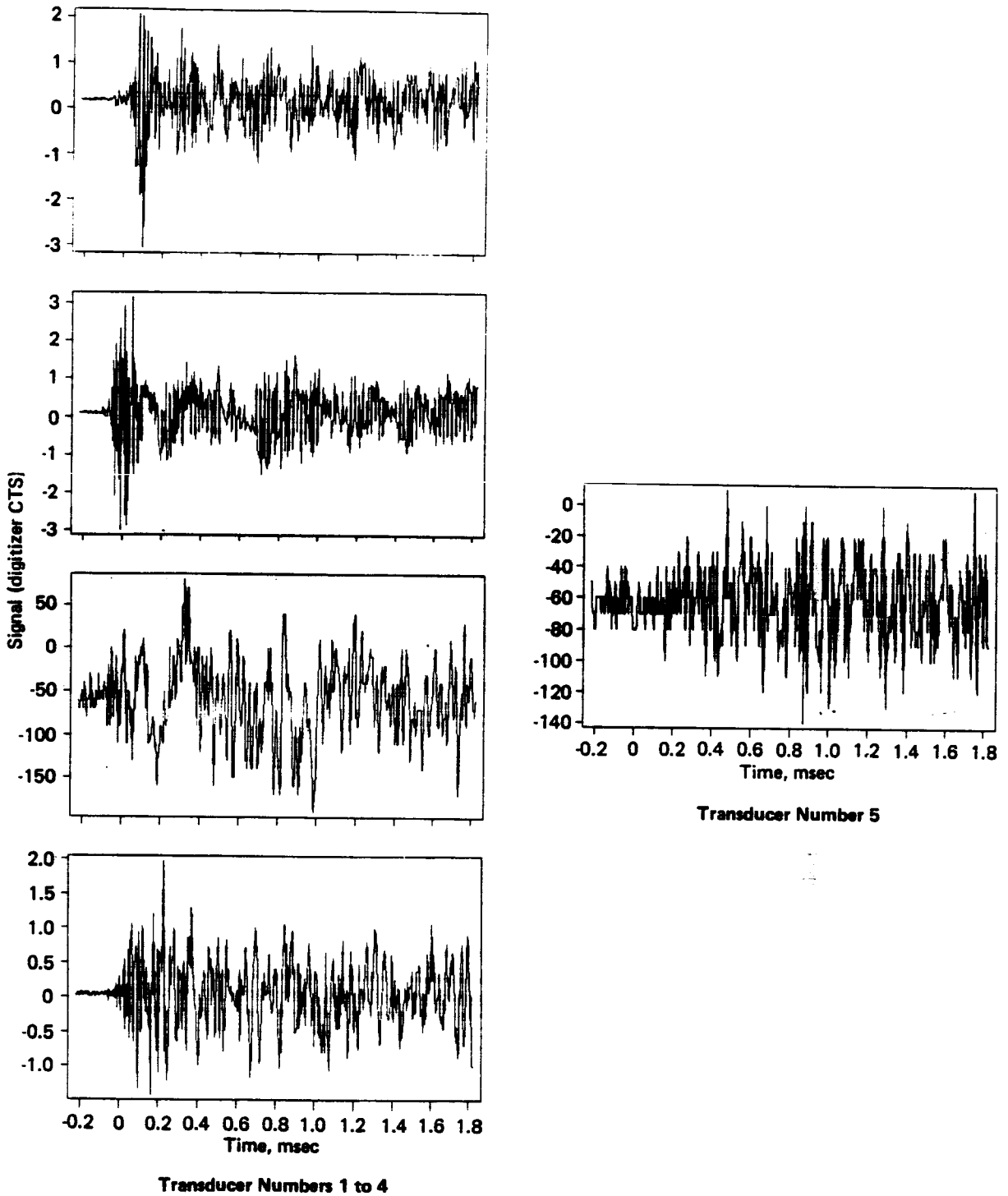
Figure A-20. Fifth Test of 04/20/87
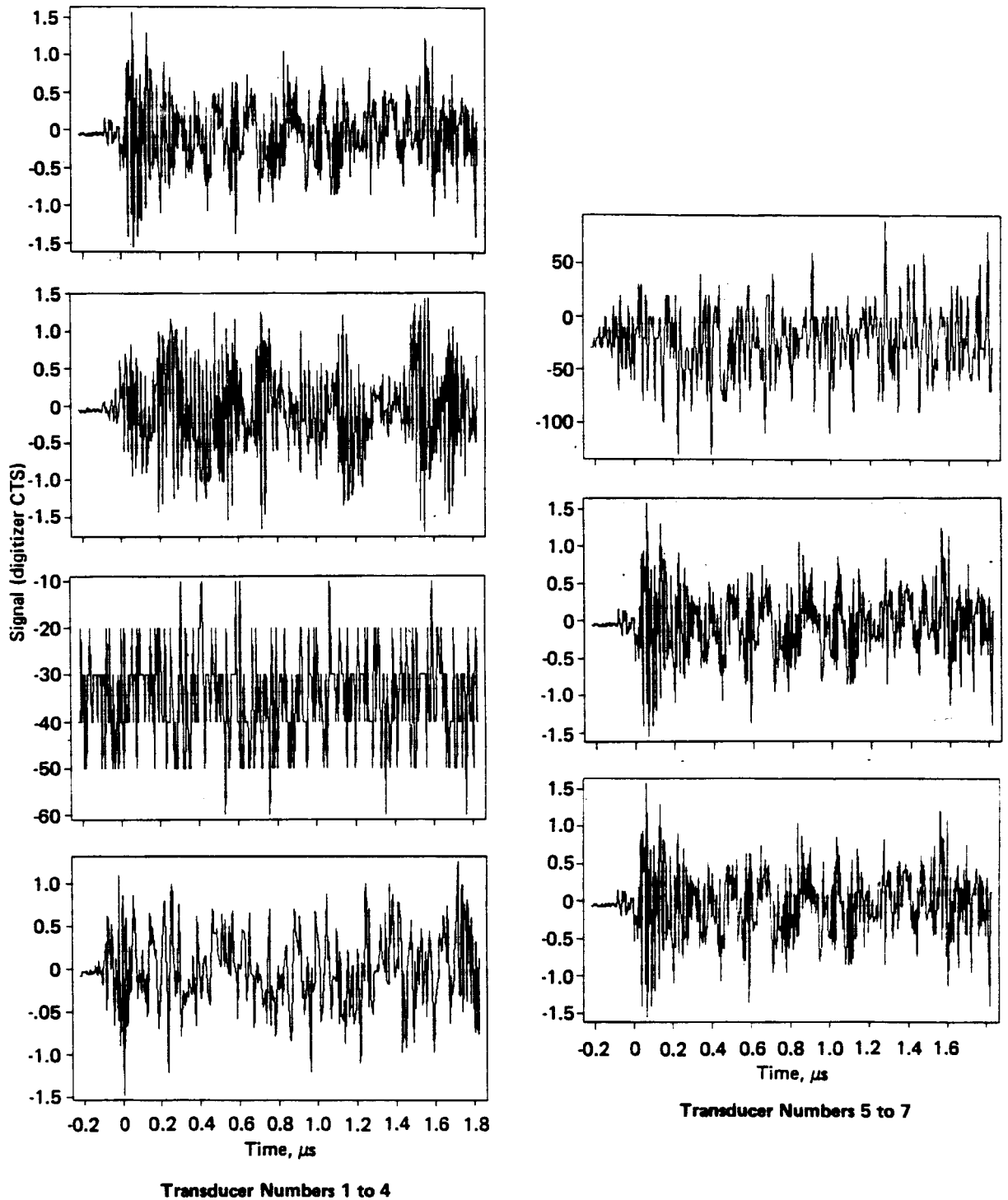
Figure A-21. Sixth Test of 04/20/87

Signal (digitizer CTS)

Time, μs

Transducer Numbers 1 to 4

Transducer Numbers 5 to 7
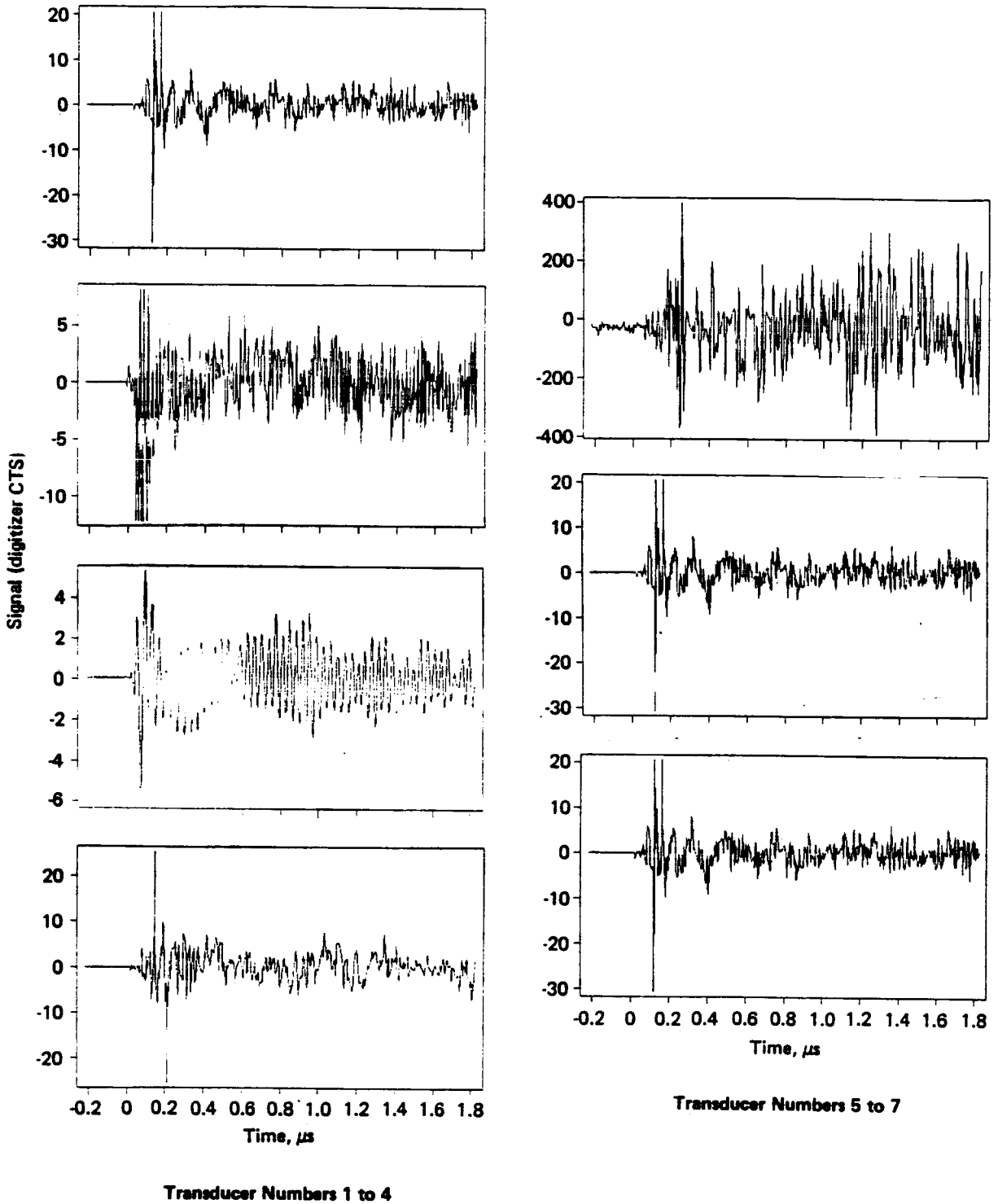
Figure A-22. First Test of 04/23/87
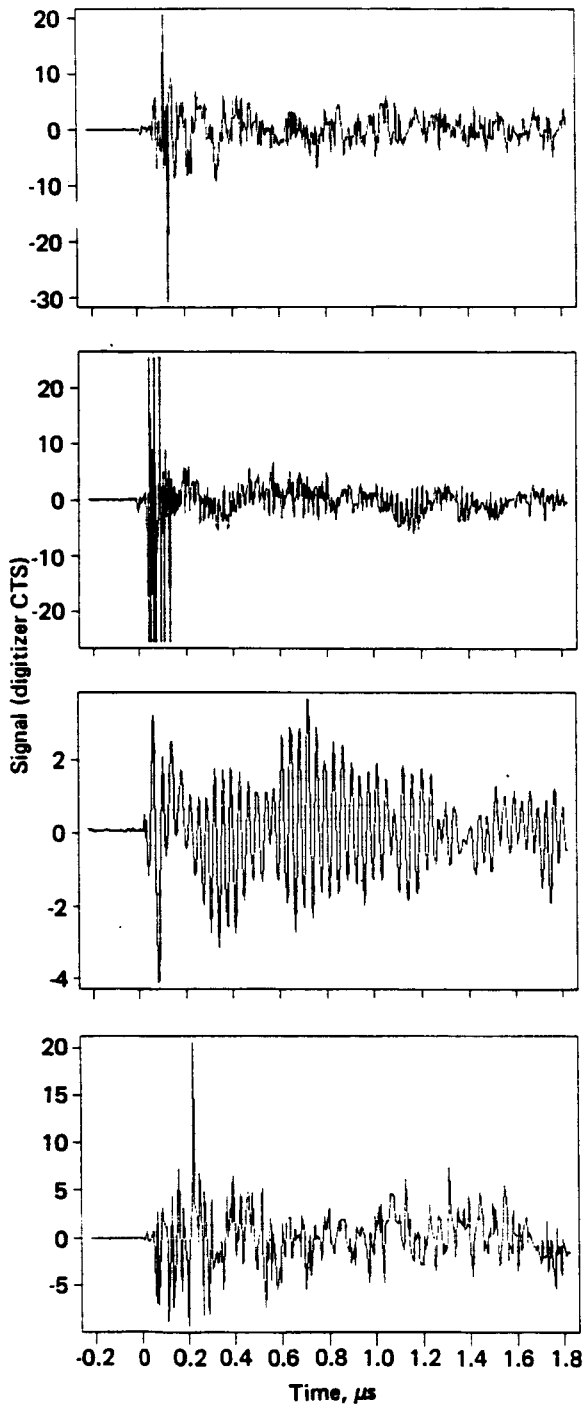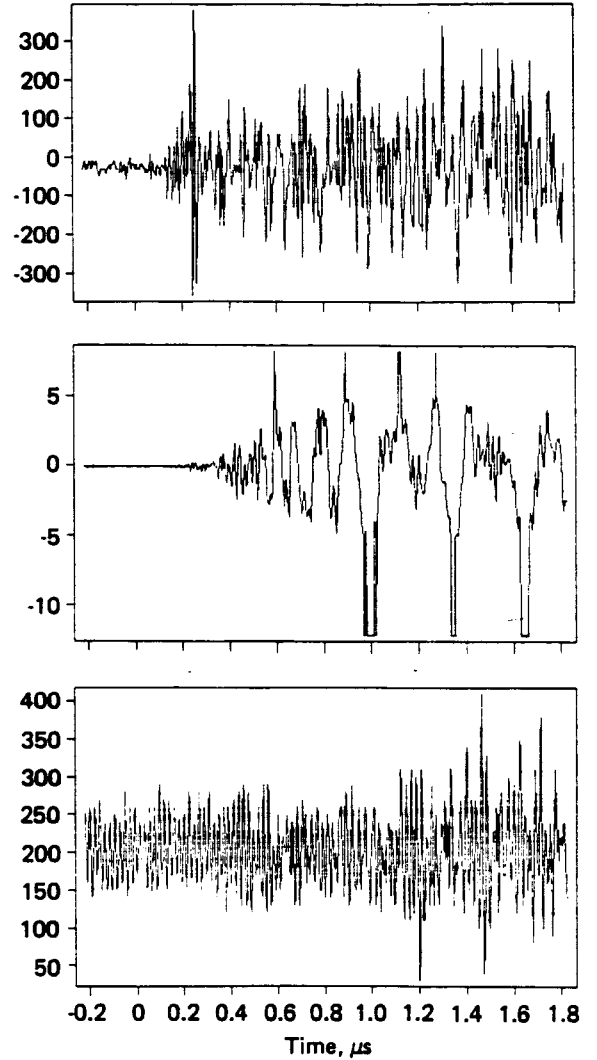
Figure A-23. Second Test of 04/23/87
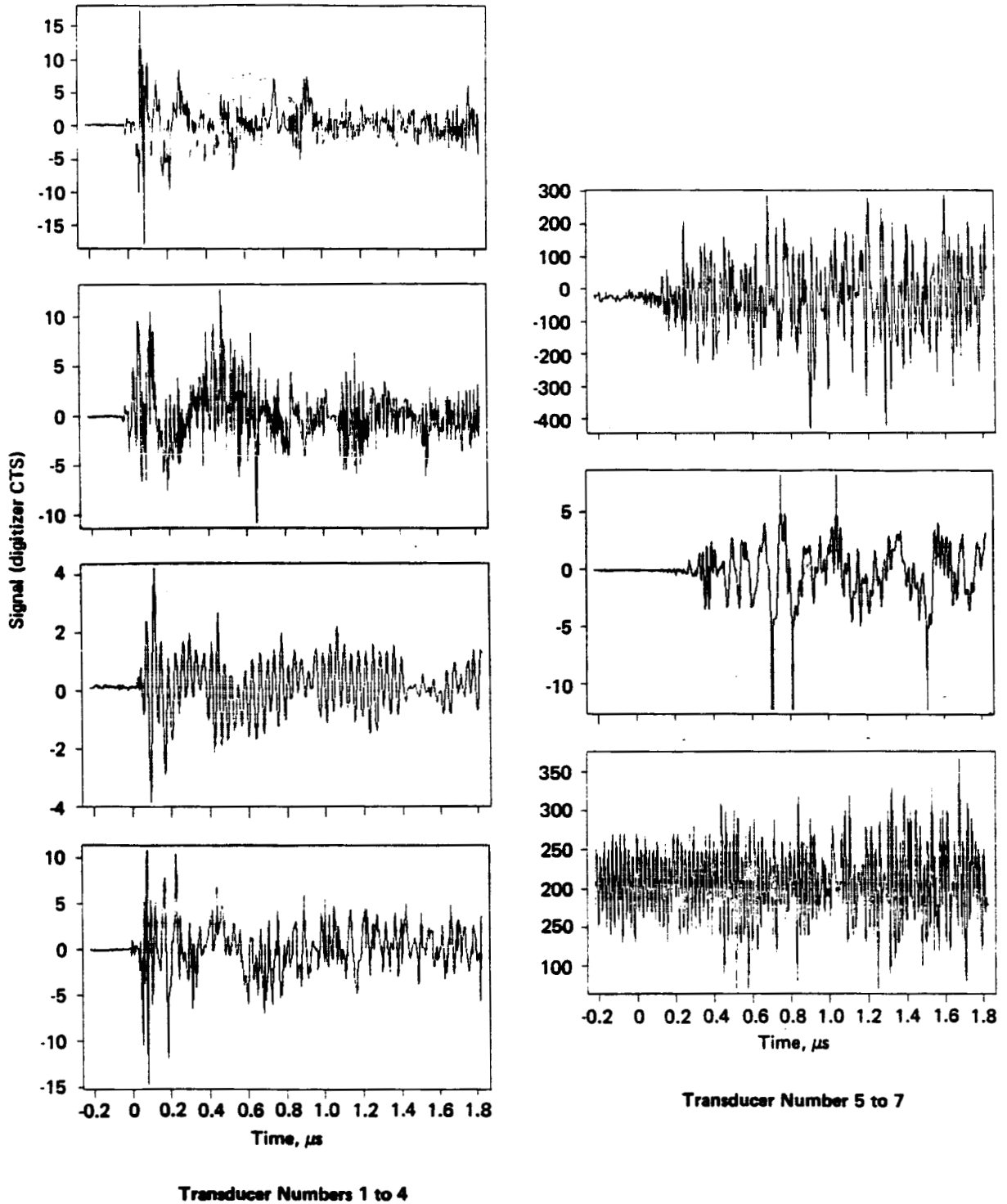
Figure A-24. Third Test of 04/23/87
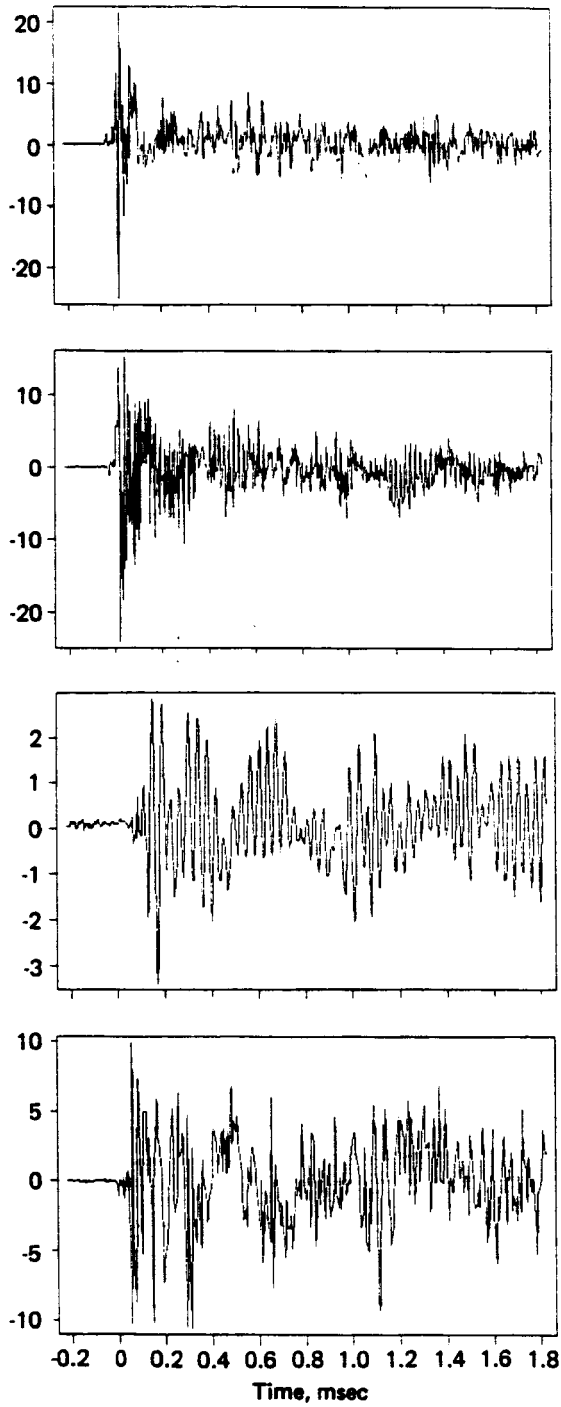
ORIGINAL PAGE IS
OF POOR QUALITY

Transducer Numbers 1 to 4
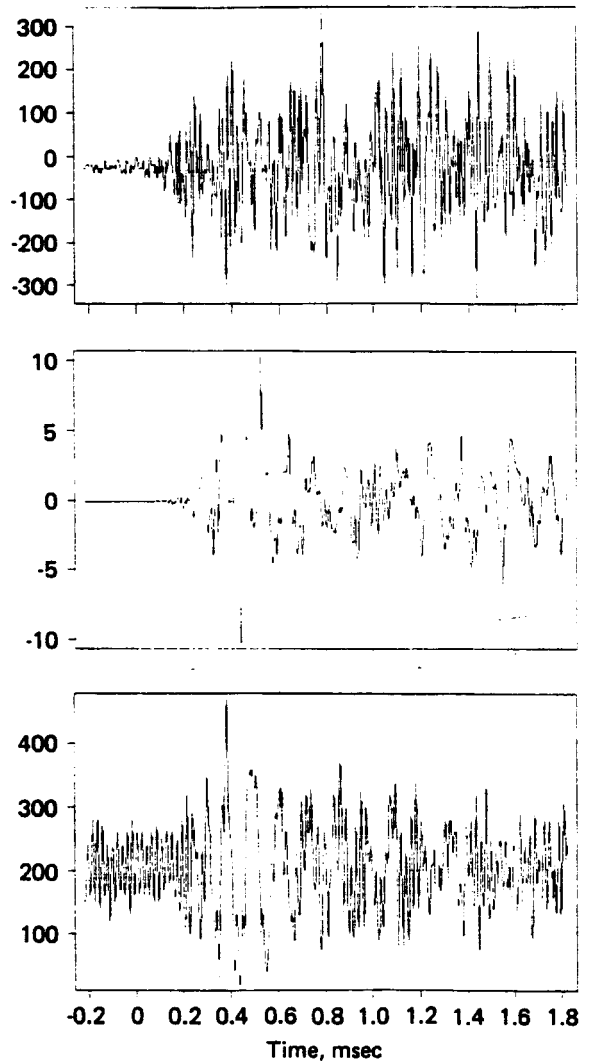
Transducer Numbers 5 to 7

Figure A-25. Fourth Test of 04/23/87

60
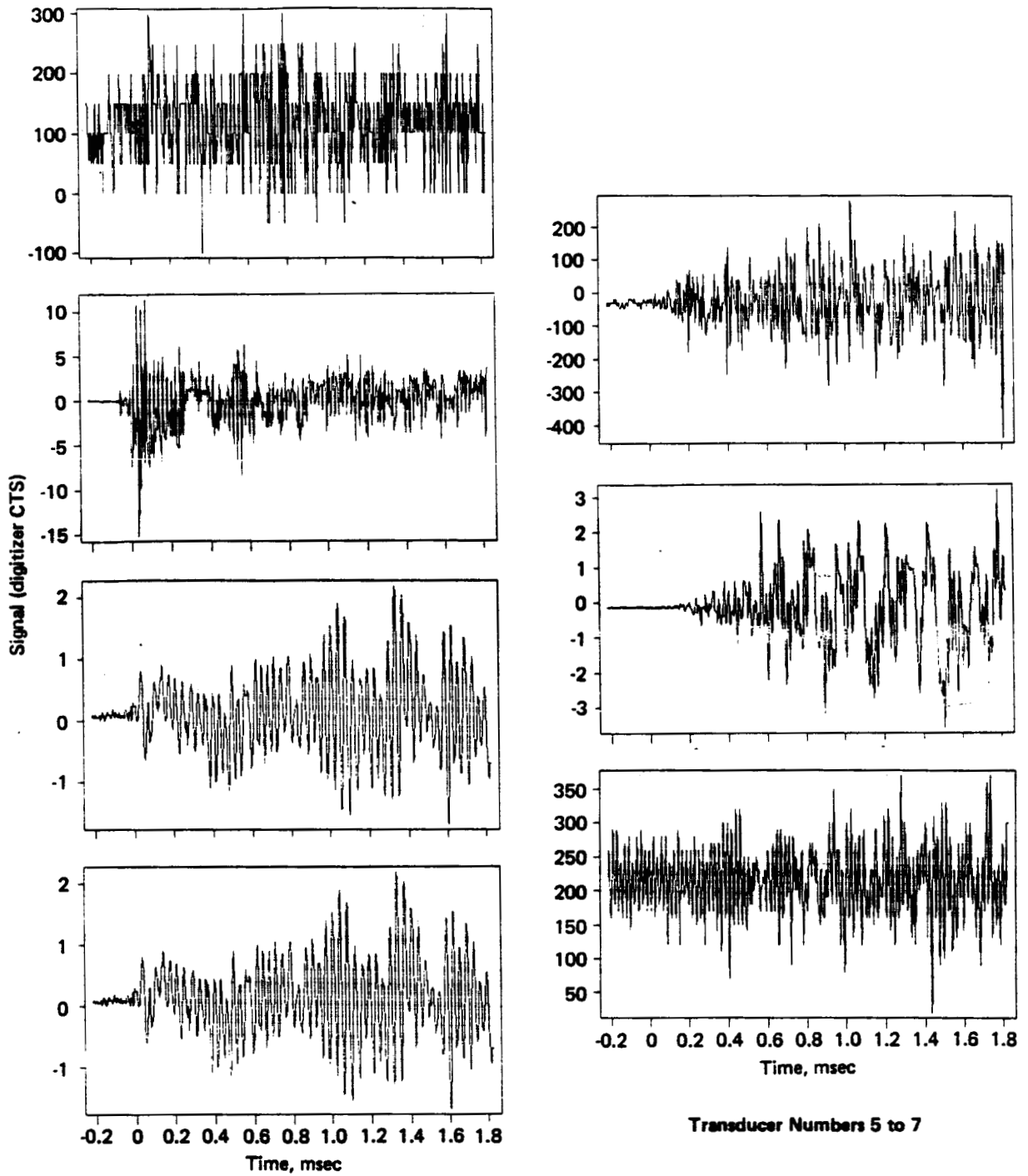
Figure A-26. Fifth Test of 04/23/87

61
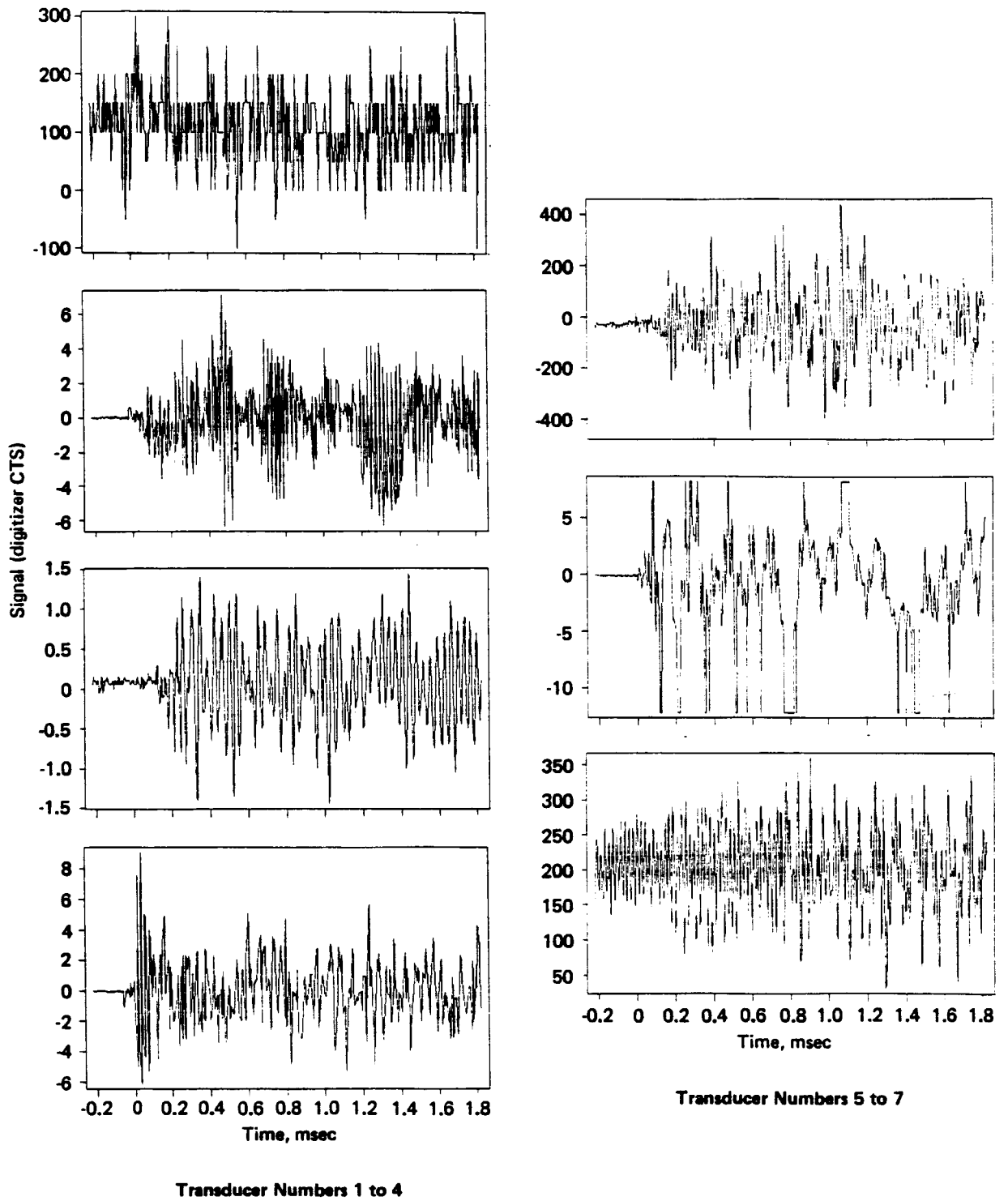
Figure A-27. Sixth Test of 04/23/87
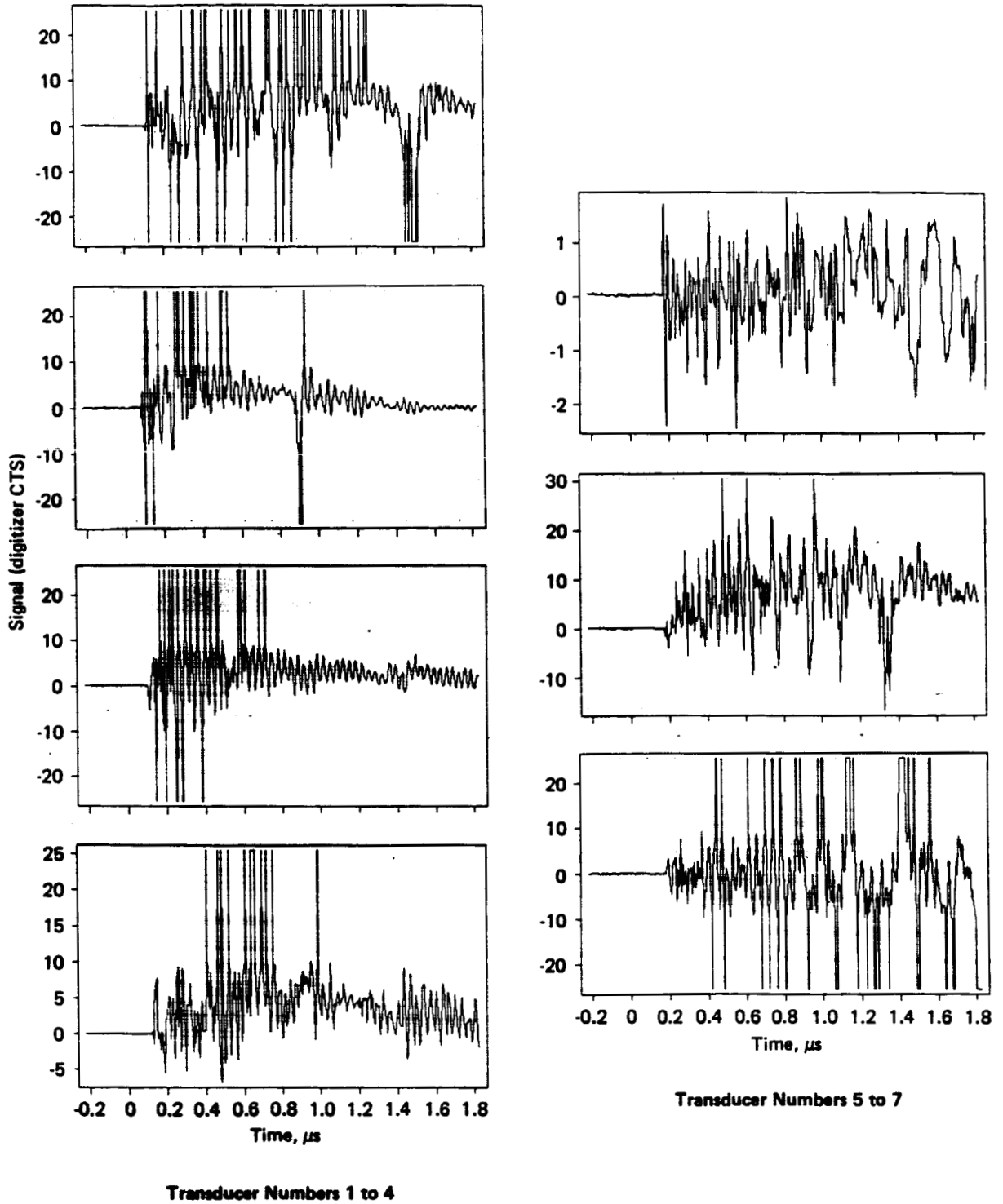
Figure A-28. First Test of 05/04/87
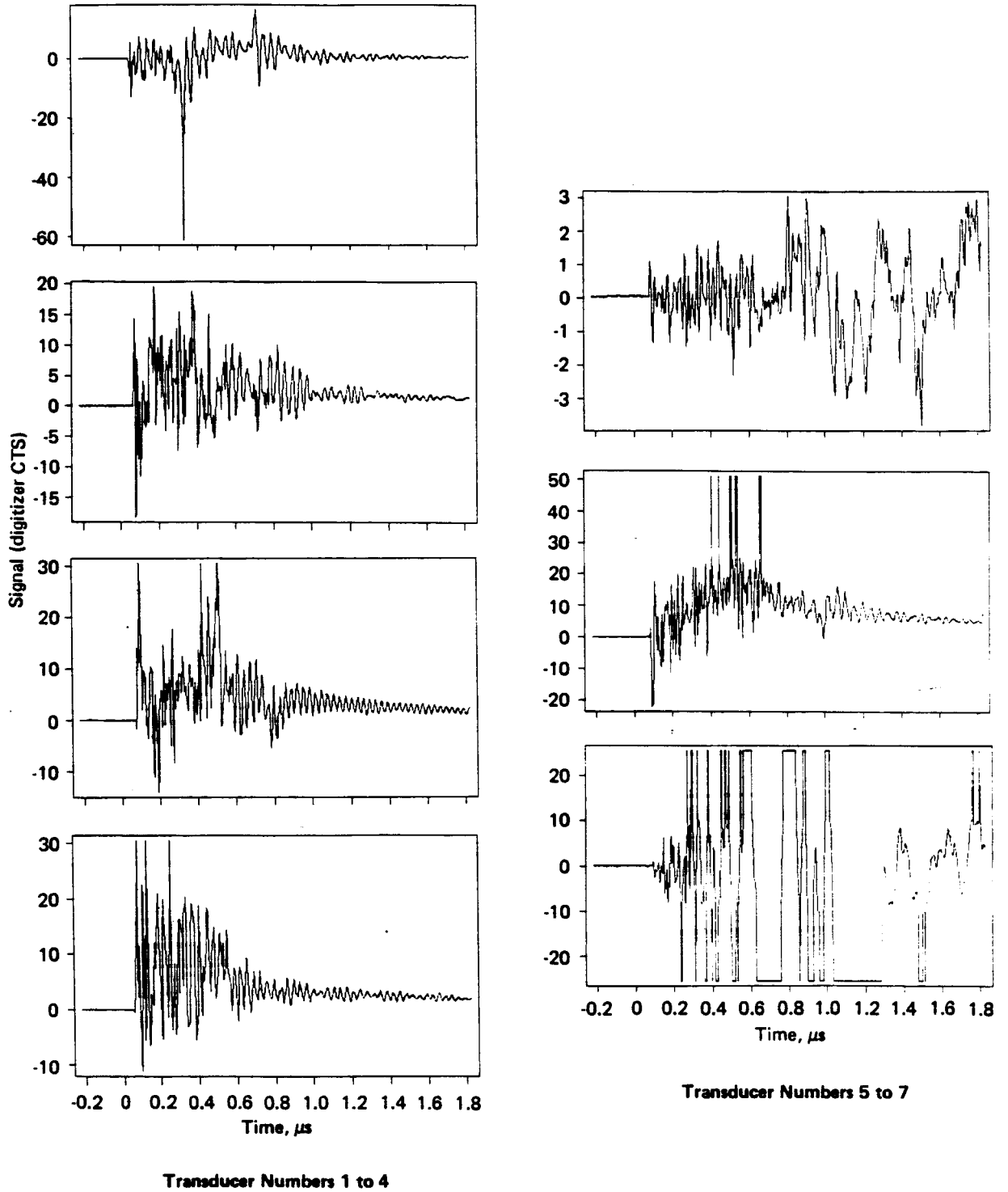
Figure A-29. Second Test of 05/04/87
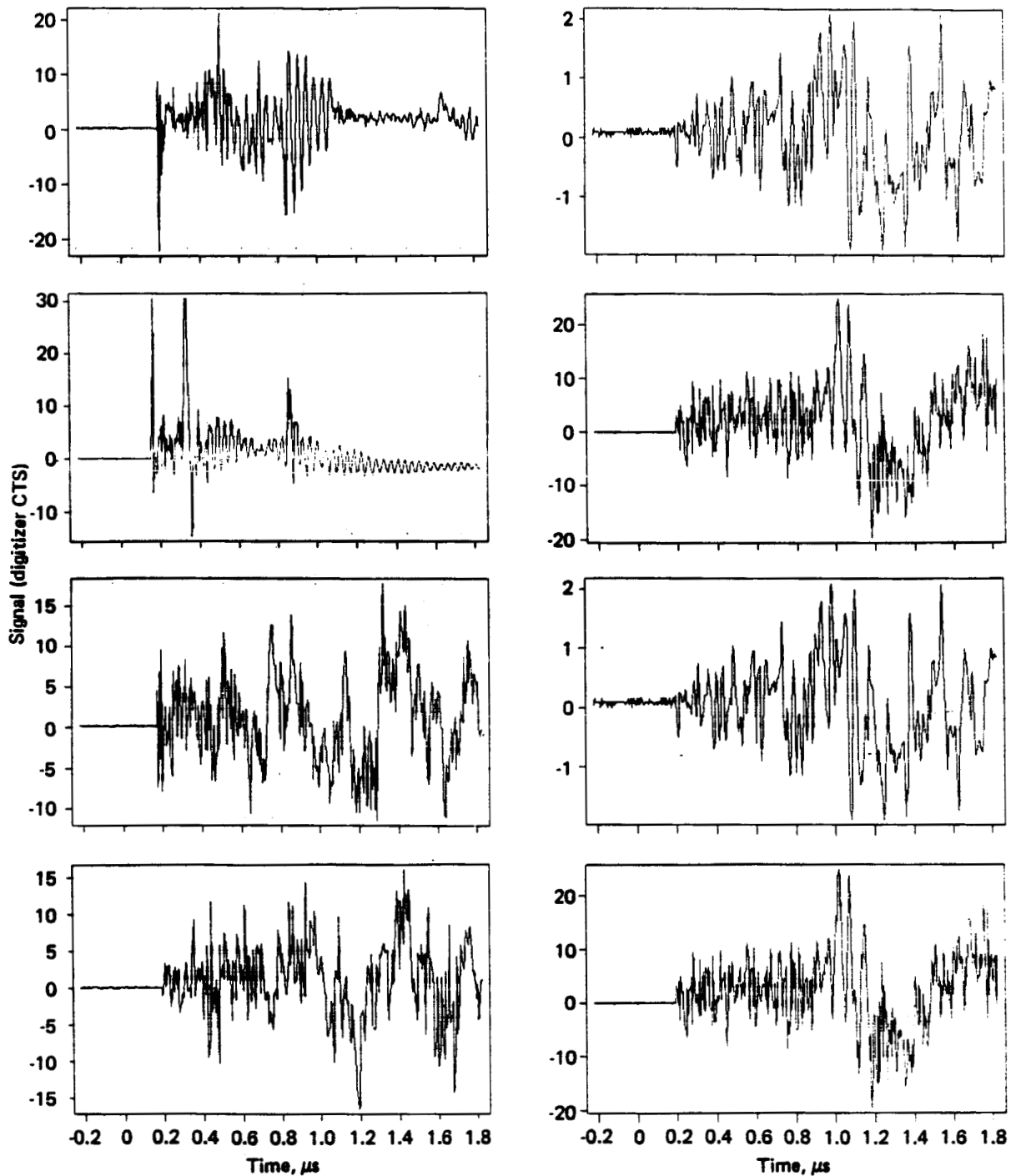
Figure A-30. First Test of 05/05/87
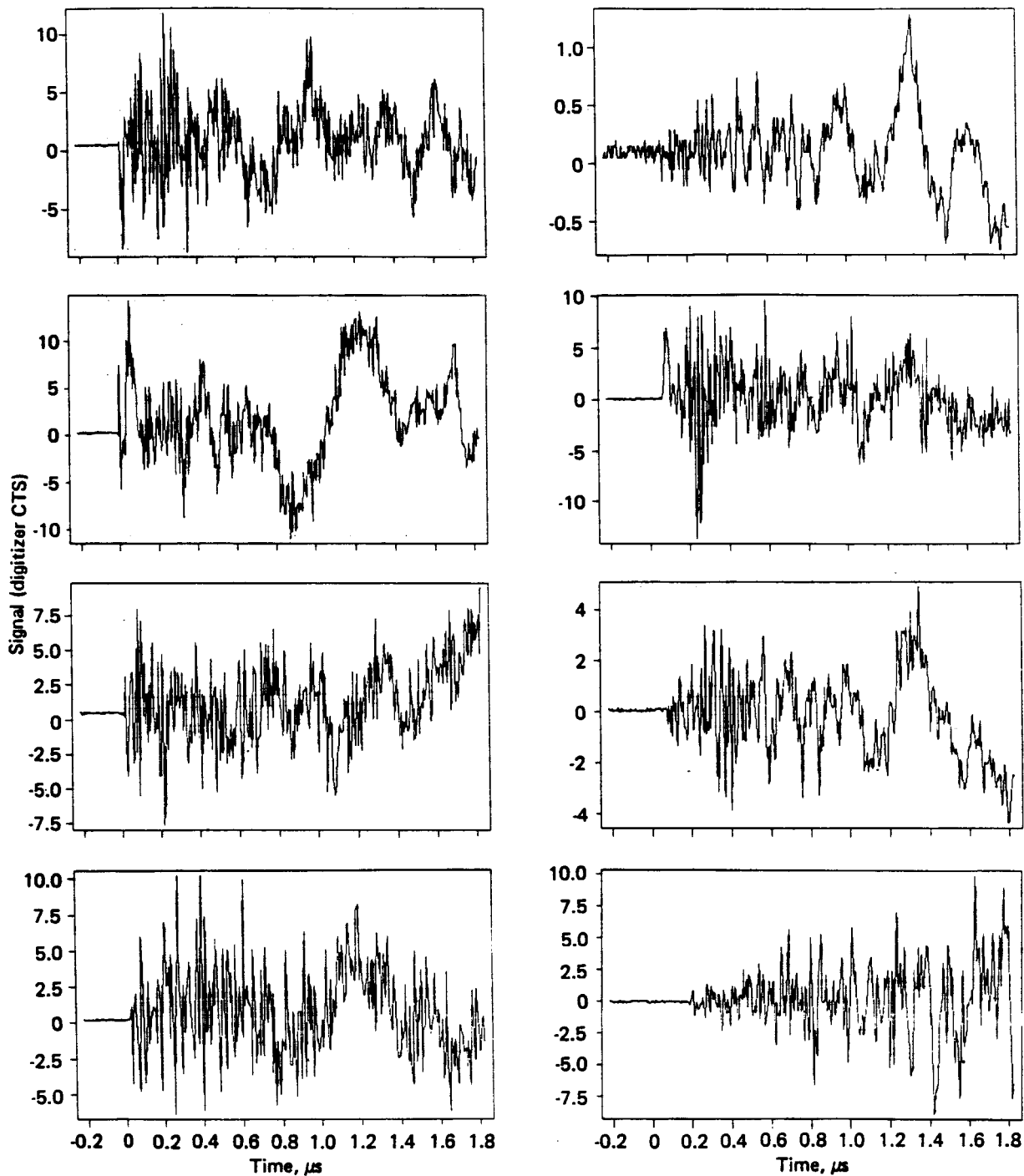
Figure A-31. Second Test of 05/06/87

66